

How to get cool in the heat: comparing analytic models of halo gas cooling with EAGLE

Adam R. H. Stevens,^{1*} Claudia del P. Lagos,^{2,3} Sergio Contreras,⁴ Darren J. Croton,¹ Nelson D. Padilla,^{4,5} Matthieu Schaller,⁶ Joop Schaye⁷ and Tom Theuns⁶

¹*Centre for Astrophysics & Supercomputing, Swinburne University of Technology, Hawthorn, VIC 3122, Australia*

²*International Centre for Radio Astronomy Research, The University of Western Australia, Crawley, WA 6009, Australia*

³*Australian Research Council Centre of Excellence for All-sky Astrophysics (CAASTRO), Redfern, NSW 2016, Australia*

⁴*Instituto de Astrofísica, Pontificia Universidad Católica de Chile, Santiago, Chile*

⁵*Centro de Astro-Ingeniería, Pontificia Universidad Católica de Chile, Santiago, Chile*

⁶*Institute for Computational Cosmology, Durham University, Durham, DH1 3LE, United Kingdom*

⁷*Leiden Observatory, Leiden University, 2300 RA Leiden, The Netherlands*

8 July 2022

ABSTRACT

We use the hydrodynamic, cosmological EAGLE simulations to investigate how hot gas in haloes condenses to form and grow galaxies. We select haloes from the simulations that are actively cooling and study the temperature, distribution, and metallicity of their hot, cold, and transitioning ‘cooling’ gas, placing these in context of semi-analytic models. Our selection criteria lead us to focus on Milky Way-like haloes. We find the hot-gas density profiles of the haloes form a progressively stronger core over time, the nature of which can be captured by a β profile that has a simple dependence on redshift. In contrast, the hot gas that actually cools is broadly consistent with a singular isothermal sphere. We find that cooling gas carries a few times the specific angular momentum of the halo and is offset in spin direction from the rest of the hot gas. The gas loses $\sim 60\%$ of its specific angular momentum during the cooling process, generally remaining greater than that of the halo, and is better aligned with the cold gas already in the disc than anything else. Angular-momentum losses are slightly larger when cooling onto dispersion-supported galaxies. We show that an exponential surface density profile for gas arriving on a disc remains a reasonable approximation, but a cusp is always present, and disc scale radii are larger than predicted by a vanilla Fall & Efstathiou model. These scale radii are still closely correlated with the halo spin parameter, for which we suggest an updated prescription for galaxy formation models.

Key words: galaxies: evolution – galaxies: formation – galaxies: haloes – ISM: evolution – ISM: structure

1 INTRODUCTION

Fundamentally, galaxies must form from the cooling and condensation of gas residing in overdense regions of the Universe (e.g. White & Rees 1978). The manner in which the gas is accreted over cosmic time is vital to the structure of a galaxy and how it evolves. This is especially true for late-type galaxies, where discs hold the majority of a galaxy’s baryonic mass, and when considering the high-redshift Universe, prior to mergers dominating the growth of the most massive galaxies.

The semi-analytic approach of galaxy formation (see White & Frenk 1991; Kauffmann, White & Guiderdoni 1993;

Kauffmann et al. 1999) provides a framework that is consistent with the hierarchical assembly of overdense regions, known as haloes. Here, the histories and properties of dark-matter haloes formed in a cosmological N -body simulation provide the input for the coupled differential equations that describe the evolution of galaxies. These computationally efficient models have proven highly successful in their ability to reproduce the statistical properties of galaxies in the local Universe and are becoming progressively more successful in the early Universe (e.g. Gonzalez-Perez et al. 2014; Henriques et al. 2015; Lacey et al. 2015).

Many of the semi-analytic models in the literature (e.g. Cole et al. 2000; Hatton et al. 2003; Croton et al. 2006, 2016; Lagos, Cora & Padilla 2008; Somerville et al. 2008b; Guo et al. 2011; Benson 2012) have been, in part, based on

* E-mail: astevens@astro.swin.edu.au

the disc formation scenario developed by [Fall & Efstathiou \(1980\)](#) and [Mo, Mao & White \(1998\)](#). In these models, it is assumed that halo gas has a uniform temperature and carries the same total specific angular momentum as the halo (variants have adopted a statistical take on spin direction – see [Padilla et al. 2014](#); [Lagos et al. 2015a](#)). Two regimes of gas accretion onto galaxies are typically employed. For the ‘hot mode’, infalling gas is first shock heated to the virial temperature, then must cool to reach the galaxy. In the ‘cold mode’, the cooling time-scale is small relative to the free-fall time-scale, and hence the former no longer sets the time-scale for accretion (see [Birnboim & Dekel 2003](#); [Kereš et al. 2005](#); [Benson & Bower 2011](#)). When the gas condenses onto a disc, it is assumed to conserve its specific angular momentum, and to settle with a surface density that decreases exponentially with radius. Often rotation curves of discs are approximated as completely flat. Variants also include exponential cooling profiles as a function of specific angular momentum ([Stevens, Croton & Mutch 2016](#)). While these assumptions all carry physical merit, like anything, they would ideally be subject to independent testing.

With this study, we are motivated to investigate the basic assumptions of the aforementioned models with respect to the hot mode of accretion. That is, how is hot gas distributed in haloes, what is the nature and distribution of gas as it cools onto a galaxy, and does this gas conserve its specific angular momentum? These are not only important science questions in and of themselves, but answers to these have a direct impact on galaxy evolution model development. To address these topics with modern observations would be an unsurmountable challenge. In this sense, we cannot *truly* test the model assumptions. We can, however, look to numerical experiments with more detailed physics for insight, namely hydrodynamic cosmological simulations. This allows us to see how the widely adopted theoretical description of gas cooling on global scales ([Fall & Efstathiou 1980](#); [White & Frenk 1991](#)) compares to predictions from modelling galaxy evolution physics on local (\lesssim kpc) scales. Hydrodynamic simulations also carry the advantage that we can immediately relate any results regarding gas cooling to the properties of dark-matter haloes.

We use the EAGLE simulations (Evolution and Assembly of GaLaxies and their Environments; [Schaye et al. 2015](#); [Crain et al. 2015](#)) to study the gas particles in haloes that cool from a hot state down onto galaxies. We assess how these particles are distributed in physical space and in terms of specific angular momentum both prior to and after cooling episodes. We compare this against the overall hot and cold gas profiles in haloes, investigating how the process of cooling leads to evolution in these structures. We further determine whether the angular momentum of these particles is conserved as they cool, both on an individual basis and as a collective system. EAGLE provides an ideal testbed to address these questions, as there is growing evidence the simulation produces a realistic galaxy population in terms of mass ([Furlong et al. 2015a](#)), size ([Furlong et al. 2015b](#)), specific angular momentum ([Lagos et al. 2016](#)), and gas content ([Lagos et al. 2015b](#); [Bahé et al. 2016](#)).

Recently, [Guo et al. \(2016\)](#) compared the galaxy populations of two semi-analytic models, run on the dark-matter-only halo merger trees of EAGLE, against the main hydrodynamic EAGLE simulation. Those authors found consis-

tency in the evolution of the stellar mass function and the specific star formation rates of galaxies, but noted clear differences when galaxies were broken into passive and star-forming. However, their study did not address whether the physical description and approximations of galaxy evolution processes in the semi-analytic models were supported by hydrodynamic simulations. Our study contributes by focussing on the physics of the models, rather than testing whether the end result, i.e. the galaxy properties, are in agreement with each other or observations.

This paper is structured as follows. In Section 2, we provide details on the design of the EAGLE simulations and the data products that we have used. We specify the sample of galaxies within the simulations that we study. In Section 3, we examine the state of hot gas in haloes, comparing this to the particles which are about to cool. In Section 4, we discuss the direction and magnitude, with respect to the halo, of the specific angular momentum of gas as it cools, and whether this is conserved. Once those particles have cooled onto a disc, we study their distribution, and that of the disc in full, in Section 5. The results of this paper are then summarised in Section 6.

Throughout this paper, where relevant, we assume the cosmology used in the EAGLE simulations (see Section 2). We also use the term ‘virial radius’ as the radius enclosing an average density 200 times greater than the critical density of the Universe. I.e. $R_{\text{vir}} = R_{200}$, $M_{\text{vir}} = M_{200} = M(< R_{200})$. We use capital R for three-dimensional radial distances ($R^2 = x^2 + y^2 + z^2$) and lower-case r for two-dimensional equivalents ($r^2 = x^2 + y^2$, where the z -direction is always parallel to the relevant rotation axis).

2 THE EAGLE SIMULATIONS AND DATA

2.1 Overview of the simulations

The EAGLE simulations are a suite of state-of-the-art hydrodynamic, cosmological simulations, first presented by [Schaye et al. \(2015\)](#). They were run using a significantly modified version of GADGET3, an N -body Tree-PM smoothed-particle hydrodynamics (SPH) code. Various modifications of GADGET have been developed by the community. The most recent official public release was GADGET2 ([Springel 2005](#)). The simulations assumed a Λ CDM cosmology with parameters based on the 2013 *Planck* data release: $\Omega_M = 0.307$, $\Omega_\Lambda = 0.693$, $\Omega_b = 0.048$, $h = 0.6777$, $\sigma_8 = 0.8288$, and $n_s = 0.9611$ ([Planck Collaboration XVI 2014](#)). The main ‘Reference’ simulation used a dark-matter particle mass of $9.70 \times 10^6 M_\odot$, an initial gas particle mass of $1.81 \times 10^6 M_\odot$, and a Plummer-equivalent gravitational softening scale of 2.66 comoving kpc for $z > 2.8$ and 700 physical pc otherwise. The simulations implemented a modified version of SPH, dubbed ANARCHY (Dalla Vecchia in preparation; but see appendix A of [Schaye et al. 2015](#)), along with the time-step limiter of [Durier & Dalla Vecchia \(2012\)](#). [Schaller et al. \(2015b\)](#) presented a comparison of the simulations with the old SPH version, and found that the modifications were important for active galactic nucleus (AGN) activity and star formation rates of large galaxies, but, by and large, did not have a big impact on stellar masses and sizes.

The simulations include a set of sub-grid models that describe physical processes below the resolution limit. These are described in full in [Schaye et al. \(2015\)](#). Briefly, these include the following.

- Radiative cooling of gas particles is calculated by following 11 elements ([Wiersma, Schaye & Smith 2009a](#)), which are assumed to be in ionization equilibrium. Gas is exposed to the cosmic microwave background, and after $z = 11.5$, a uniform ionizing background is included ([Haardt & Madau 2001](#)). Self-shielding and local stellar radiation are ignored.
- Star formation is based on the local pressure of gas ([Schaye & Dalla Vecchia 2008](#)) and is consistent with the Kennicutt-Schmidt relation ([Kennicutt 1998](#)). This is only triggered above a threshold local density, which has a metallicity-dependent value ([Schaye 2004](#)). Star particles are each considered to be single stellar populations that follow the initial mass function of [Chabrier \(2003\)](#) and the stellar evolution models described by [Wiersma et al. \(2009b\)](#). Stellar feedback from supernovae is implemented with the stochastic thermal model of [Dalla Vecchia & Schaye \(2012\)](#).
- Black-hole particles of mass $10^5 h^{-1} M_\odot$ are seeded in haloes once they reach a mass of $10^{10} h^{-1} M_\odot$ ([Springel, Di Matteo & Hernquist 2005](#)). These accrete gas from neighbouring particles, with consideration of angular momentum as in [Rosas-Guevara et al. \(2015\)](#), which leads to AGN feedback where nearby gas particles are stochastically heated ([Schaye et al. 2015](#)).

The free parameters of the sub-grid physics in EAGLE were calibrated to best reproduce a small number of key observables of galaxies in the local ($z \sim 0$) Universe: the stellar mass function ([Li & White 2009](#); [Baldry et al. 2012](#)), the stellar size–mass relation of [Shen et al. \(2003\)](#), and the black hole–stellar mass relation of [McConnell & Ma \(2013\)](#). See [Crain et al. \(2015\)](#) for further details.

In this paper, in addition to the Reference simulation, we also use runs with modified feedback physics but equal resolution. These include runs with stellar feedback half the Reference strength (WeakFB), stellar feedback with twice the Reference strength (StrongFB), and an absence of active galactic nucleus feedback (NoAGN). We also use the high-resolution run of EAGLE (with 8-fold superior mass resolution), for which the strength of feedback was recalibrated to meet the same observational constraints as mentioned above (RecalHR). The alternate-feedback and high-resolution runs were performed in 25-Mpc boxes. As we want to fairly compare these to Reference haloes, we use the 25-Mpc Reference simulation for this paper as well. Further details on these simulations can also be found in [Crain et al. \(2015\)](#).

2.2 Halo finding

To identify structures in EAGLE, SUBFIND ([Springel et al. 2001](#); [Dolag et al. 2009](#)) was run on the output of the simulations. For the purposes of the code, a ‘halo’ is a collection of particles found with a friends-of-friends algorithm. A ‘subhalo’ is a set of particles in a halo which is enclosed by isodensity contours that traverse saddle points, where only particles gravitationally bound to the substructure are included. A subhalo encompasses a galaxy and its immediate surroundings. All haloes have a minimum of one subhalo

(haloes with more than one subhalo have satellite galaxies). Neither haloes nor subhaloes are inherently restricted to their virial radii (we specify when only particles within R_{vir} are considered). Note that all results in this paper concerning ‘haloes’ only consider the primary subhalo.

2.3 Galaxy sample selection

For the purposes of this paper, we are interested in studying haloes undergoing cooling episodes. To identify a relevant sample of systems in EAGLE, first we select central subhaloes (most massive in their parent halo) with total gas masses $> 10^{9.5} M_\odot$, then we compare the state of gas particles of the same IDs at temporally adjacent snapshots within each subhalo. More specifically, we take each relevant subhalo at snapshot number s and tabulate the IDs of all particles we consider ‘hot’. We then find the same particles at snapshot $s + 1$ and determine which of these are now ‘cold’ and within the same system. Those that have transitioned from hot to cold, or from hot to a star particle, from snapshot s to $s + 1$ are labelled ‘cooled’ particles. Equivalently, we refer to these as ‘cooling’ particles at snapshot s . If the number of cooling particles exceeds a threshold value (64, see below), then we deem a resolved cooling episode to have happened and include that subhalo in our sample. We perform this same process for all snapshot pairs.

Note that in order to have a clean sample of central galaxies to compare against how semi-analytic models treat centrals, we exclude galaxies from our analysis that are satellites at either snapshot (that is, we only consider the primary subhalo of each halo). We further exclude galaxies that undergo a major merger between snapshots. We define a major merger as one where the smaller galaxy has a stellar mass at least 30% that of the central. These would have only constituted a small fraction of our sample. As such, had we included them, our results would not have noticeably changed. When selecting haloes from the alternate-feedback and high-resolution runs, we add a requirement that only haloes also present in the Reference sample can be included.

Throughout this text, we define ‘cold’ particles as either having non-zero star formation rates or having both temperature $T < 10^{4.5} \text{ K}$ and hydrogen number density $n_H > 0.01 \text{ cm}^{-3}$, which should capture the interstellar medium of most galaxies. Conversely, ‘hot’ gas particles have zero star formation rates and $T > 10^5 \text{ K}$.

A cooling episode should occur over a time-span comparable to the dynamical time of a halo, which is directly tied to the Hubble flow at the given redshift:

$$t_{\text{dyn}} = R_{\text{vir}}/V_{\text{vir}} = [10 H(z)]^{-1}, \quad (1)$$

where R_{vir} and V_{vir} are the virial radius and velocity, respectively, of a given halo. As we want to capture the before and after states of a cooling episode, snapshots separated by a dynamical time would be well suited for our study. By no coincidence, the temporal separation between snapshots in EAGLE is always within 40% of a dynamical time (with the exception of the first two snapshots in the simulation, which we do not use in this paper). This is illustrated by Fig. 1.

The precise threshold imposed for the minimum number of cooling particles is, at some level, arbitrary. A threshold is required to avoid numerical noise and to ensure a meaningful mass cools. We find a round value of 64 particles returns

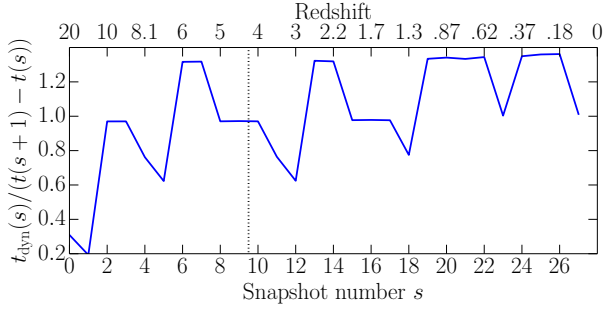


Figure 1: Ratio of a halo dynamical time at the redshift of snapshot number s to the time to the next snapshot in EAGLE. Snapshots to the right of the vertical dotted line were included in the analysis of this paper.

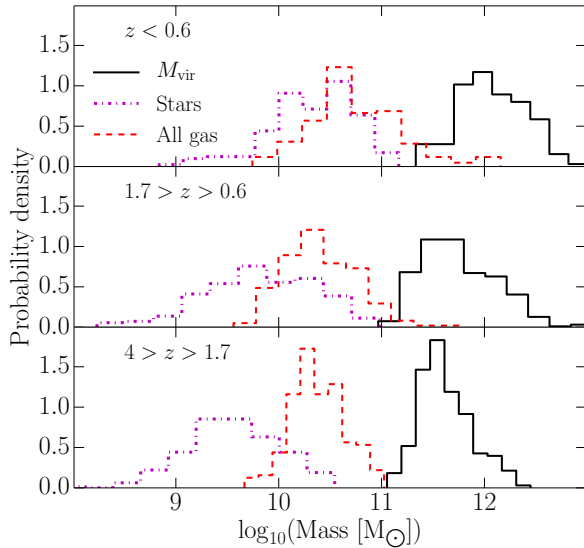


Figure 2: Normalised histograms of masses of Reference EAGLE systems used in this paper, according to the selection criteria given in Section 2.3. The solid distributions give the haloes’ virial masses. The dashed and dot-dashed distributions give the gas and stellar masses, respectively, of all particles in the main subhalo within R_{vir} . Each panel covers a different redshift range, as labelled, with the same number of snapshots.

a sizeable number of haloes (an average of 48 per snapshot interval in the 25-Mpc box), each with sizeable cooling rates ($\gtrsim 0.2 M_{\odot} \text{ yr}^{-1}$). As will be shown, this threshold leads to results that are consistent with the RecalHR simulation when we select the same haloes. We are, however, restricted to studying haloes at $z < 4$. The average temporal separation between snapshots in this range is 681 Myr.

We present the masses of our sample of Reference EAGLE haloes in Fig. 2. We break these into three redshift bins, each with 6 snapshot pairs, which we use throughout the paper. The normalised histograms show the virial masses of the haloes, as well as the gas and stellar masses of all particles in each respective main subhalo inside an aperture of R_{vir} . Note that the gas masses are for *all* gas, i.e. hot + cold + everything in between.

3 BEFORE COOLING: HOT GAS IN HALOES

3.1 Temperature profiles of hot gas

In the absence of cold streams, before finding itself in a galaxy, gas will find itself in a hot state, sitting in a halo. Models of galaxy evolution often operate under the assumption that hot gas in haloes, and therefore hot gas that will cool, carries a uniform temperature that is equal to the virial temperature. To compare against this, we examine the temperature profiles of haloes in our EAGLE sample, each normalised by its virial temperature. The virial temperature is given by

$$T_{\text{vir}} = \frac{\bar{\mu} m_p}{2k_B} V_{\text{vir}}^2 = 35.9 \left(\frac{V_{\text{vir}}}{\text{km s}^{-1}} \right)^2 \text{ K}, \quad (2)$$

where k_B is the Boltzmann constant, and we have adopted a mean molecular weight, $\bar{\mu} m_p$, of 59% that of the proton mass.

We present temperature profiles of hot gas from our sample of EAGLE haloes from the Reference and RecalHR runs in the top panels of Fig. 3. The profiles were built by measuring the mean temperature of hot gas particles within spherical shells. We use (a maximum of) 100 shells for each halo, where each shell encompasses the same number of particles for a given halo, unless that width is below the spatial resolution (softening scale) of the simulation. We show the evolution of these profiles by grouping systems into three redshift bins, where each bin includes the same number of snapshots. We display profiles for the median and 16th–84th percentile range of our samples in Fig. 3. It is immediately clear that the hot gas is not truly isothermal, but rather temperature tends to decrease with radius. At higher redshift, the gas is within a factor of ~ 2 of being isothermal and only approaches T_{vir} towards the centre. As time evolves, the centres become hotter and the temperature gradient steepens.

The bottom panels in Fig. 3 consider only the hot gas that will cool onto the galaxy before the subsequent snapshot, which we dub ‘cooling’ particles. As these particles only constitute a small fraction of the hot gas, we reduce the number of spherical shells to 20 in each halo for measuring these profiles. $T_{\text{cooling}}(R)$ has a clear gradient from high redshift onward. This shows that gas that settles onto a galaxy from a larger distance tends to already be cooler than the inner gas. Physically, this makes sense, as gas at large radii is at lower density (see below) and hence has less opportunity to lose its energy through collisions over the same time. It is not surprising that the average temperature of cooling gas is consistently below the hot gas in general; the hotter particles would require longer to cool. Perhaps what is more interesting is that as the centres of haloes heat overall, the temperature of the *cooling* particles *decreases*. Feedback processes lead to energy being transferred out of the galaxy, raising the mean temperature at the centre of the hot halo. This reheated gas takes time to mix with its surroundings and/or cool back onto the galaxy. Meanwhile, the gas that was already in the process of cooling continues to cool, and is evidently oblivious to the heating of its surroundings. Small differences are seen between the Reference and RecalHR runs (which we come back to briefly in Section 4.2), but they are broadly consistent with each other.

To better quantify the effect of feedback, we have

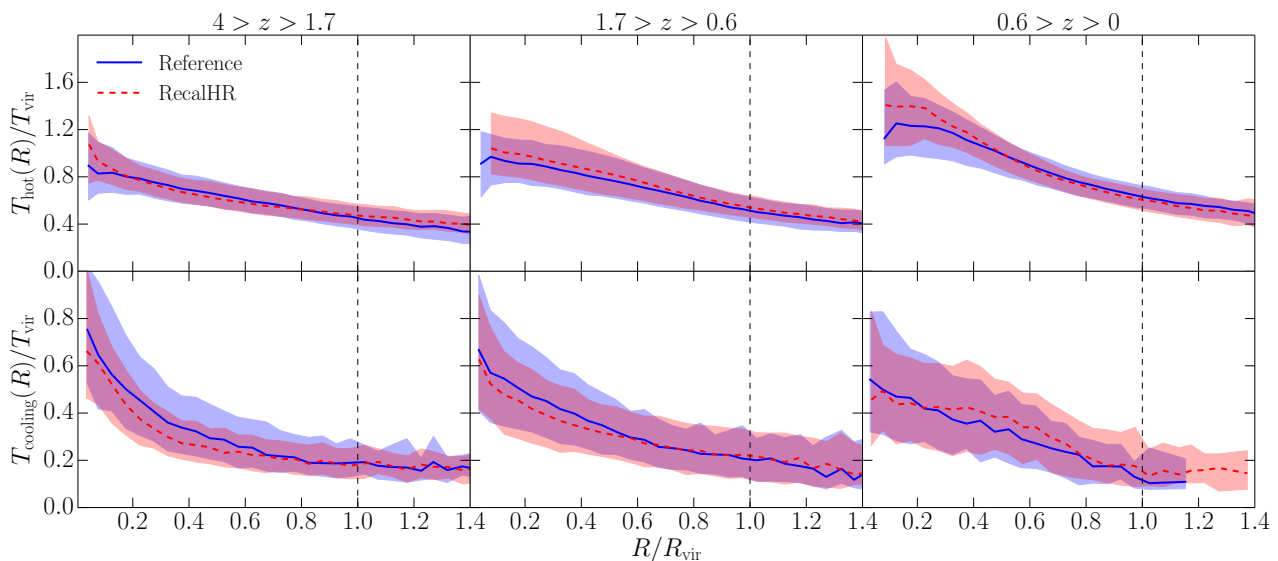


Figure 3: Temperature profiles of non-star-forming, hot ($T > 10^5$ K) gas in haloes in the Reference and RecalHR runs of EAGLE. The top row of panels presents the temperature profiles for *all* hot gas in the haloes, while the bottom panels only include hot gas particles that are known to cool onto the galaxy by the following snapshot. The temperature in both these cases is normalised by the virial temperature of each halo. Columns of panels are for different redshift ranges. The median (solid and dashed curves) and inner 68% (shaded regions of corresponding colour) of profiles are shown in each panel for the two simulations. Vertical dashed lines are given at R_{vir} to indicate the cut-off for what is typically regarded as part of a halo. While the hot-gas temperature rises in the centre, the gas that cools continues to get cooler.

produced the same temperature profiles for the alternate-feedback runs of EAGLE. We present these for the lowest redshift bin in Fig. 4, comparing the median profile of the Reference simulation to the median, 16th and 84th percentiles of the WeakFB, StrongFB and NoAGN runs. At higher redshift, the profiles of the alternate-feedback runs more closely matched those of the Reference run (as they have the same initial conditions). The differences seen at low redshift are hence directly the result of feedback associated with galaxy evolution. Note that the number of systems meeting our selection criteria in each run varies as a result of the differing feedback. These numbers are given in the legend of Fig. 4.

Let us first examine the role of stellar feedback. Stellar feedback is implemented thermally in EAGLE. This raises the temperature of gas particles in the centre of the haloes, where the exploding stars are. These hot particles rise and can drive shocks that heat their neighbours. In our sample, the masses of the haloes are large enough that supernova energy is insufficient to eject gas from galaxies out of the halo entirely. The result instead is that the gradient of the temperature profile becomes generally steeper. Both the $T_{\text{cooling}}(R)$ and $T_{\text{hot}}(R)$ profiles for the WeakFB run lie below the Reference curves, as one would expect from having less heating. For the StrongFB run, the rise of $T_{\text{hot}}(R)$ is even more stark than the Reference run, yet the median $T_{\text{cooling}}(R)$ profile *matches* the Reference simulation. This supports the argument raised above that while stellar feedback affects the mean temperature of halo gas, it does not immediately impact the gas already in the process of cooling.

Let us now consider the role of AGN. Perhaps counter-intuitively, switching AGN off leads to an evolution in $T_{\text{hot}}(R)$ that looks similar to the StrongFB case. While AGN

feedback does heat the central gas particles in a halo, the net effect is less a case of the temperature simply rising at the centre, and more a case of AGNs regulating the temperature of the gas throughout the haloes. Strong outflows from AGNs advect hot particles to larger distances from the galaxy than stellar-driven outflows would, thereby spreading the heat out and reducing the gradient. The difference between the NoAGN run and the others is that $T_{\text{cooling}}(R)$ has also increased throughout the halo. This shows that an AGN suppresses the ability of hot gas to cool, rather than directly heating gas, as now, without AGN, hotter gas is seen to cool more efficiently. This is precisely how radio mode AGN feedback is considered in semi-analytic models (e.g. Bower et al. 2006; Croton et al. 2006); that is, the heating rate of a radio AGN is subtracted directly off the cooling rate of a halo to calculate its net cooling rate (see Appendix A). Although, note that EAGLE does not distinguish between radio and quasar modes of AGN, instead opting for a single model of AGN feedback which is more in line with the quasar mode (see Schaye et al. 2015). Even if the net effect of AGN feedback in EAGLE is to make the cooling process less efficient, one would expect the properties of AGN-driven winds in EAGLE to differ if radio mode feedback were implemented directly in the simulation (see Dubois et al. 2012).

3.2 Density profiles of hot gas

We now turn our attention to the density profiles of hot gas in haloes. Using the same spherical shells as used for the temperature profiles, we measure the density within each shell of our EAGLE haloes. We normalise the density profile of each hot halo by $m_{\text{hot}}/R_{\text{vir}}^3$. We then make the same measurements for the cooling gas, instead normalised by $m_{\text{cooling}}/R_{\text{vir}}^3$. This allows us to directly compare the den-

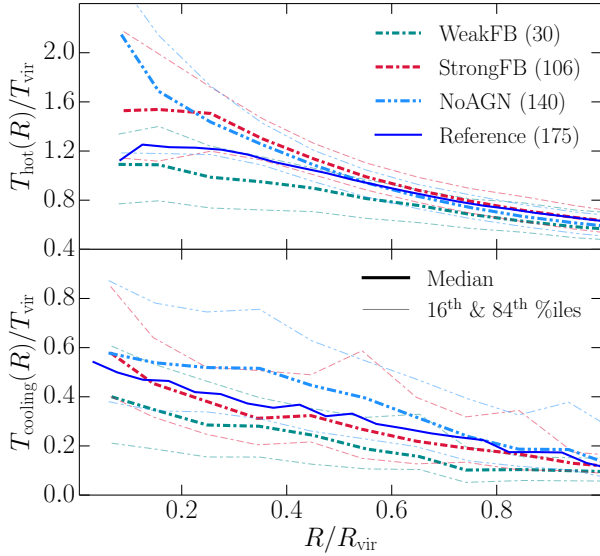


Figure 4: Temperature profiles of hot gas in haloes for various alternate-feedback runs of EAGLE, only considering systems at $z < 0.6$. The top panel includes all hot gas in the profiles, while the bottom panel only includes that which is known to cool before the next time-step. The thick, opaque curves give the median profiles of the different EAGLE runs. The thin, transparent lines give the 16th and 84th percentiles for the alternate-feedback runs. The bracketed numbers in the legend indicate the number of haloes in the sample of each run. Both stellar and AGN feedback affect the temperature profiles of hot haloes, but the gas in the process of cooling is not affected identically.

sity profiles of both the hot and cooling gas, regardless of the halo size or total hot/cooling mass. In Fig. 5, we present these for the same 3 redshift bins as before. The top row shows the density profiles for all hot gas, while the bottom row is for cooling gas. The Reference and RecalHR runs produce consistent profiles (as do the alternate-feedback runs, but these are not included for clarity).

A clear evolution is seen in the hot gas density profiles, where the gradient at the centre becomes shallower with time. The cooling gas density profile evolves less noticeably, however. This is consistent with our findings for the temperature evolution. That is, while the hot gas at the centre becomes hotter and less dense (relative to the outer parts of the same halo) from supernovae and stellar winds, the gas that actually cools is almost unaffected by the feedback.

Some models of galaxy formation assume hot gas follows the density profile of a singular isothermal sphere (e.g. Croton et al. 2006, 2016; Lagos et al. 2008; Somerville et al. 2008b; Lee & Yi 2013; Stevens et al. 2016), where

$$\rho_{\text{hot}}(R) = \frac{m_{\text{hot}}}{4\pi R_{\text{vir}} R^2}. \quad (3)$$

This relation is over-plotted in each relevant panel in Fig. 5. This profile is based primarily on simplicity, where there is an absence of cited, explicit physical motivation in the models. An alternative, motivated by both theory and observations of galaxy groups and clusters, is a β profile (see the review by Mulchaey 2000). This has been incorporated in the GALFORM family of models (e.g. Cole et al. 2000; Benson et al. 2003; Font et al. 2008). The β profile prescribes

the gas density as

$$\rho_{\text{hot}}(R) = \rho_0 \left[1 + \left(\frac{R}{R_c} \right)^2 \right]^{-3\beta/2}, \quad (4)$$

where ρ_0 is the central density and R_c is a core radius. Under the assumption that all haloes follow the same value of β and that $R_c = c_\beta R_{\text{vir}}$, where c_β is a constant (e.g., as assumed by Benson et al. 2003), we can compare our EAGLE profiles to the β profile. Taking $\beta = 2/3$, the expression becomes

$$\rho_{\text{hot}}(R) = \frac{m_{\text{hot}}}{4\pi c_\beta^2 R_{\text{vir}}^3} \left[1 - c_\beta \tan^{-1} \left(\frac{1}{c_\beta} \right) \right]^{-1} \left[1 + \left(\frac{R}{c_\beta R_{\text{vir}}} \right)^2 \right]^{-1}. \quad (5)$$

Using the median density profiles of the Reference simulation in Fig. 5, we have fitted for c_β and over-plotted for comparison.

Fig. 5 clearly shows that singular isothermal spheres are not representative of the distribution of hot gas in our haloes. While the $\rho_{\text{cooling}}(R)$ profiles are closer to being exponential on average than anything else, curiously, they do encompass the singular isothermal sphere profile within their 68% confidence range, at least for $z > 0.6$. A singular isothermal sphere describes the cooling gas density profile as well as a best-fitting β profile would (i.e. the best-fitting c_β is large). Despite not actually having isothermal haloes, the manner in which gas cools onto galaxies in EAGLE is consistent with randomly drawing particles out of a singular isothermal sphere, which we have found is true for the alternate-feedback EAGLE runs as well (not shown here).

A β profile captures the total hot-gas density reasonably well out to $\sim 0.8 R_{\text{vir}}$, when c_β is free, as seen in the top panels of Fig. 5. By allowing this, we find the best-fitting c_β decreases with time. To quantify this, we have fitted c_β to each hot-gas density profile of our sample haloes for each snapshot individually. We have done this for the Reference, RecalHR, and alternate-feedback EAGLE runs, and present the evolution of c_β for these in Fig. 6. We include the median relation for all runs, and include the scatter for the Reference simulation. We find that weak stellar feedback can affect the value of c_β at $z \lesssim 1$, but otherwise the fit is fairly robust to feedback changes. In addition, we find the median $c_\beta(z)$ curve for the Reference simulation is fitted almost perfectly by a simple analytic expression:

$$c_\beta(z) \simeq 0.21e^{-1.5z} - 0.036z + 0.27. \quad (6)$$

This least-squares fit (which weights each snapshot equally) is included in Fig. 6. We note that for all $z < 4$, the best-fitting c_β is above the values assumed in previous incarnations of GALFORM: 0.07 (Benson et al. 2003) and 0.1 (Font et al. 2008).

3.3 Metallicity profiles of hot gas

Another common approximation made in analytic models is that the metallicity of hot gas is uniform throughout the halo. In reality, we would expect hot gas at the centre of haloes to be more metal-rich than at the outskirts, as the stars at the bottom of the potential well are what produce new metals. To demonstrate the degree to which this is true

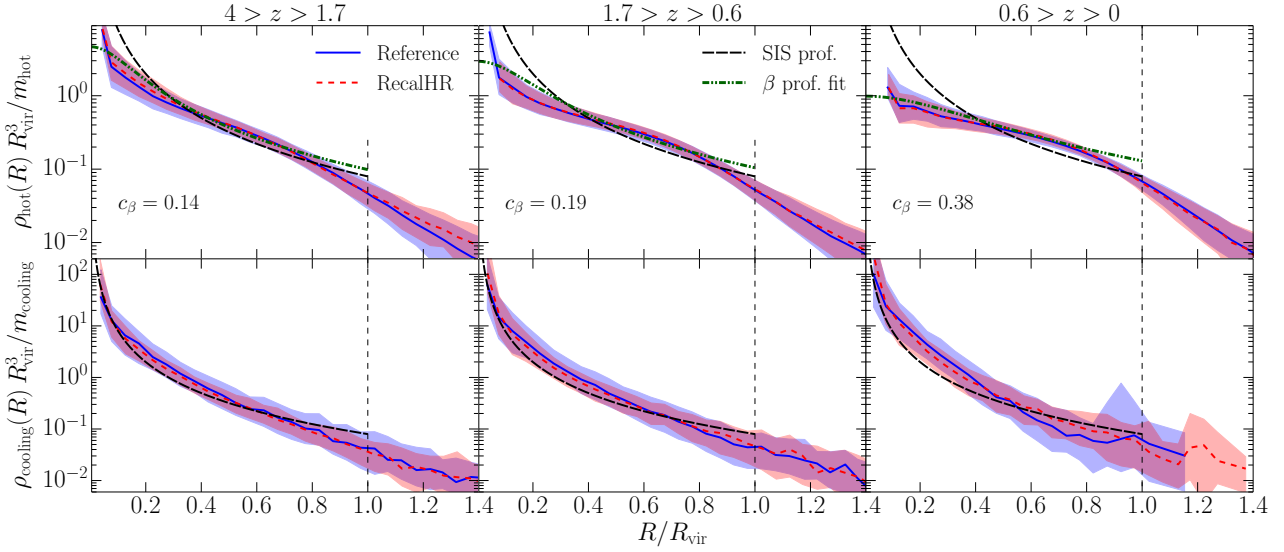


Figure 5: As for Fig. 3 but instead showing density profiles of hot and cooling gas, normalised by the average density within R_{vir} . These are compared against a singular isothermal sphere profile in all panels, and against a β profile for all hot gas, which is fitted to median density profile of the Reference simulation in each case. The numbers in the bottom left of those panels give the value of c_β for the fit (see equation 5). A fitted β profile describes the hot gas as a whole reasonably well, yet the gas that cools is roughly consistent with a singular isothermal sphere.

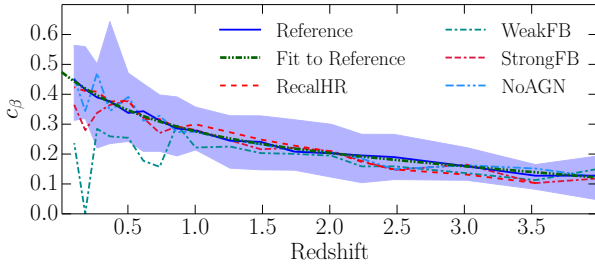


Figure 6: Best-fitting concentration parameter of β profile fits to the hot-gas density profiles of haloes in our EAGLE sample at each snapshot, assuming $\beta = 2/3$, for various runs as given in the legend. Each curve gives the median relation from each simulation, with the exception of the perfectly smooth curve, which is a fit to the Reference simulation median (equation 6), which happens to describe many of the other runs well too. The shaded region covers the 16th–84th percentile range for the Reference simulation.

for EAGLE, we calculate the mass-weighted mean metal fraction of particles in each spherical shell (as defined in Section 3.1) of each halo, and plot the normalised metal fraction profiles of our sample haloes at $z < 0.6$ in Fig. 7. We include the median and 16th–84th percentile range for the Reference, WeakFB, and StrongFB simulations. At higher redshift, the behaviour of these three simulations is similar to the Reference case presented at low redshift, and thus these have been omitted for simplicity. The RecalHR simulation is also consistent with the Reference case presented here, and is omitted for clarity. In all cases, we find metallicity becomes increasingly variant towards the centres of haloes, with a general trend of metallicity increasing. The effect of stellar feedback enriching the hot halo is clear; by $z < 0.6$, the centres of haloes in the StrongFB simulation have the steepest gradients, and the WeakFB simulation the

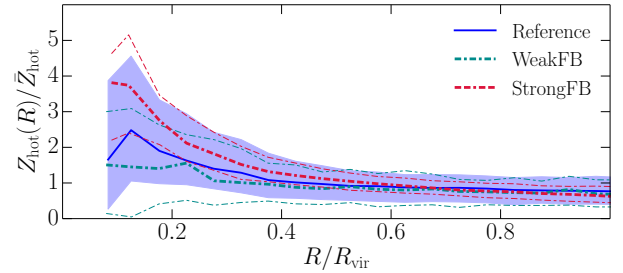


Figure 7: Metal fraction profiles for hot gas in our EAGLE haloes at $z < 0.6$, normalised by the average metal fraction in each case. The thick curves give the median for each labelled simulation. The shaded region covers the 16th–84th percentile range for the Reference simulation, while the thin curves cover the same range for the WeakFB and StrongFB runs. Stellar feedback is seen to enrich the centres of hot haloes with metals.

shallowest. As the rate at which gas cools is dependent on metallicity, metallicity gradients can have an impact on the cooling calculation in a semi-analytic model, which we turn our attention to next.

3.4 Cooling time profiles

The primary purpose of semi-analytic models including prescriptions for the hot-gas density profile, temperature, and metallicity is to determine a cooling rate at each time-step. It is, therefore, of interest what consequences will arise for the cooling rates from the differences in the profiles of the EAGLE haloes versus analytic approximations. To investigate this, we must first address the typical process for calculating cooling rates in semi-analytic models.

The majority of semi-analytic models (e.g. Cole et al. 2000; Hatton et al. 2003; Cora 2006; Croton et al. 2006, 2016; Somerville et al. 2008b; Guo et al. 2011; Lee & Yi 2013)

calculate cooling rates using some variation of the method presented in [White & Frenk \(1991\)](#), which is as follows (but see, e.g., [Monaco et al. 2007](#) for a more detailed treatment). Given a spherically symmetric distribution of hot gas, the ‘cooling time’ for hot gas at a given radius is first defined as

$$t_{\text{cool}}(R) \equiv \frac{3}{2} \frac{T_{\text{hot}}(R)}{\rho_{\text{hot}}(R)} \frac{\bar{\mu} m_p k_B}{\Lambda(T_{\text{hot}}(R), Z_{\text{hot}}(R))}, \quad (7)$$

where $\Lambda(T, Z)$ is the cooling function, commonly drawn from the tables of [Sutherland & Dopita \(1993\)](#), dependent on the temperature and metallicity of the gas. One then defines the ‘cooling radius’, R_{cool} , as the radius at which the cooling time equals a relevant time-scale. For the purposes of this paper, we have chosen to equate this time-scale to the dynamical time, in line with the SAGE family of models ([Croton et al. 2016](#); [Stevens et al. 2016](#); [Tonini et al. 2016](#)), but this could have been informed by the free-fall time-scale instead, as in GALFORM, for example. The general argument then is that the cooling mass that crosses R_{cool} is approximately equal to the cold-gas mass deposition rate onto the galaxy ([Bertschinger 1989](#)). From this continuity law, one can calculate the rate at which gas cools onto the galaxy as

$$\dot{m}_{\text{cool, model}} = 4\pi \rho_{\text{hot}}(R_{\text{cool}}) R_{\text{cool}}^2 \left(\frac{dt_{\text{cool}}}{dR} \Big|_{R \rightarrow R_{\text{cool}}} \right)^{-1}. \quad (8)$$

In the case where $R_{\text{cool}} > R_{\text{vir}}$, haloes are assumed to be in a cold-accretion regime in a semi-analytic model, where the cooling rate is then taken as the ratio of the hot mass to the dynamical (or free-fall) time. We remind the reader that our EAGLE haloes are selected to be in the hot mode of accretion.

Our intent here is *not* to compare the true cooling rates of EAGLE haloes to those inferred by equation (8). To make that comparison would require a complete deconstruction of how feedback influences cooling in both EAGLE and in semi-analytic models. This is non-trivial, as the way in which feedback and cooling are handled in semi-analytic models is not directly comparable to what goes on in a hydrodynamic simulation, and there is plenty of variation amongst models as well (see [Lu et al. 2011](#)). A model can have degeneracies when it comes to cooling and heating rates, where the free parameters governing these are only really constrained in a relative sense, such that the *net* growth of (sometimes just the stellar content of) galaxies is representative of the observed Universe. This is why many semi-analytic-hydrodynamic comparison projects have excluded feedback (and sometimes even star formation) from the simulations entirely ([Benson et al. 2001](#); [Yoshida et al. 2002](#); [Helly et al. 2003](#); [Cattaneo et al. 2007](#); [Viola et al. 2008](#); [Saro et al. 2010](#)). What we aim to address here is how the cooling time profiles, through equation (7), vary when we include the detail of the density, temperature, and metallicity profiles we have available to us from EAGLE. In Appendix A, we go one step further, and calculate how the $t_{\text{cool}}(R)$ profiles of our EAGLE haloes would translate into an effective semi-analytic cooling rate.

It is normal for the purposes of a semi-analytic model to simplify equation (7) by taking T_{vir} as the temperature for all hot gas in the halo, and assuming all hot gas to have

the same metallicity. This then leaves $t_{\text{cool}}(R)$ for a given halo dependent on the assumed density profile. We address the impact of the density profile on $t_{\text{cool}}(R)$ in Fig. 8. The long-dashed and dot-dashed curves give the median $t_{\text{cool}}(R)$ profiles after using analytic profiles of a singular isothermal sphere and β profiles with $c_\beta = 0.1$ and $c_\beta(z)$ from equation (6), respectively. These profiles differ little, where the β fit only makes a notable difference for $R \lesssim 0.3R_{\text{vir}}$ at low redshift, where it is generally true that $t_{\text{cool}} < t_{\text{dyn}}$. As a result, the cooling radii calculated from these density profiles are all consistent. This is shown by the horizontal lines in Fig. 8, which cover the 16th–84th percentile range for $R_{\text{cool}}/R_{\text{vir}}$ in each case, with the intersecting vertical marks giving the medians.

As a direct comparison to the analytic profiles, we calculate $t_{\text{cool}}(R)$ using the actual density profiles from each Reference EAGLE halo, while maintaining the use of $T_{\text{hot}}(R) = T_{\text{vir}}$ and $Z_{\text{hot}}(R) = Z_{\text{hot}}$. The median profile (dotted curves in Fig. 8) is consistent with the analytic cases in the outer parts of the halo, but diverges for $R \lesssim 0.4R_{\text{vir}}$ for all $z < 4$ (the scatter in all these cases is consistent, but this is not shown for clarity). As a result, the cooling radii are systematically lower than their analytic counterparts. This highlights the fact that, even when using a density profile that fits the general population by construction, it is difficult to recover the true cooling radii of haloes from a hydrodynamic simulation.

Next, we consider the role of the temperature profiles of the EAGLE haloes on $t_{\text{cool}}(R)$. We again solve equation (7) with $Z_{\text{hot}}(R) = \bar{Z}_{\text{hot}}$, but use the actual profiles of the haloes for $T_{\text{hot}}(R)$ and $\rho_{\text{hot}}(R)$. The median $t_{\text{cool}}(R)$ profile in this case is given by the short-dashed curves in Fig. 8. Comparing this to the dotted curves, we see the profile flattens, which leads to a much broader range in cooling radii for the haloes. Even though a typical EAGLE halo will only have a radial variation in its temperature around a factor of 3 (cf. Fig. 3), this temperature structure can significantly impact the $t_{\text{cool}}(R)$ profile one infers for a halo, and therefore would impact the cooling rate one would determine in a semi-analytic model.

As a final step, we include the metallicity profiles of the EAGLE haloes and recalculate $t_{\text{cool}}(R)$. We include the median relation with the solid curves, and the 16th–84th percentile range with the shaded region in each panel of Fig. 8. The addition of the $Z_{\text{hot}}(R)$ profile restores sensible cooling radii values that are consistent with the haloes being in the hot mode of accretion. For completeness then, a model of halo gas that includes temperature structure should also include metallicity structure for the sake of calculating cooling radii and rates. For $z > 0.6$, these cooling radii are in moderate agreement with the purely analytic profiles. The $t_{\text{cool}}(R)$ profiles flatten at low redshift, which leads to a broad range in cooling radii, which become systematically less than the cases of the analytic profiles.

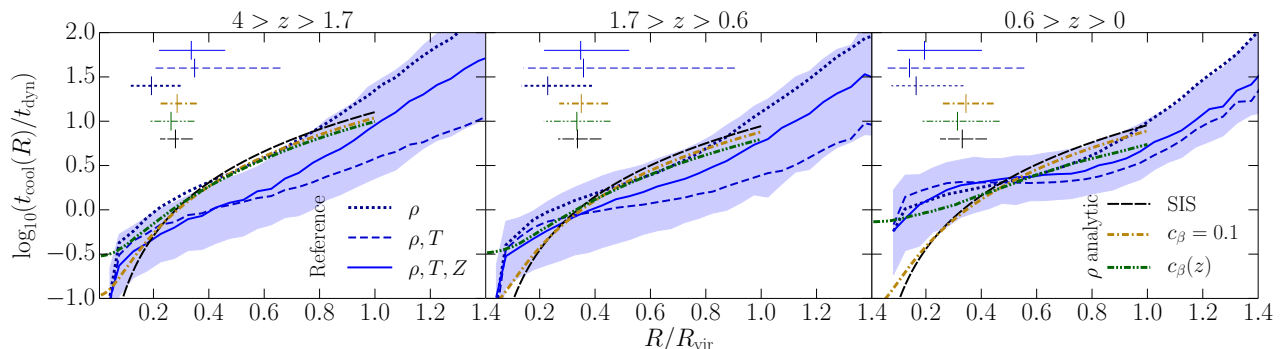


Figure 8: Cooling time of hot gas in our EAGLE halo sample, normalised by their respective dynamical times, as a function of radius, normalised by their virial radii. We present median profiles calculated from the EAGLE haloes through equation (7) in cases where we consider (i) only the density profiles of the halo with $T_{\text{hot}}(R) = T_{\text{vir}}$ and $Z_{\text{hot}}(R) = \bar{Z}_{\text{hot}}$ (dotted curves), (ii) both the density and temperature profiles with $Z_{\text{hot}}(R) = \bar{Z}_{\text{hot}}$ (short-dashed curves), and (iii) the density, temperature, and metallicity profiles of the haloes (solid curves). In the latter case, we show the 16th–84th percentile range with the shaded region. Included for comparison are the median cooling time profiles when assuming the density profile follows (i) a singular isothermal sphere, (ii) a β profile with constant $c_\beta = 0.1$, and (iii) a β profile with c_β calculated from equation (6), which take $T_{\text{hot}}(R) = T_{\text{vir}}$ and $Z_{\text{hot}}(R) = \bar{Z}_{\text{hot}}$ in all 3 cases (see the legend in the right-hand panel). The horizontal lines cover the inner 68% of $R_{\text{cool}}/R_{\text{vir}}$ values in each case, with matching linestyles. The vertical marks through these give the median cooling radii. Complete information on the density, temperature, and/or metallicity profiles of hot haloes leads to a greater range of cooling profiles than analytic approximations would give, which can impact cooling radii, thereby affecting the cooling rates one would calculate in a semi-analytic model.

4 ANGULAR MOMENTUM OF COOLING GAS

4.1 Conservation of angular momentum during cooling

An important aspect of most models of gas cooling is the assumption that the angular momentum of the gas is conserved. Of course, cooling gas can exchange angular momentum with many other parts of the halo in principle, especially through collisions with gas particles not involved in cooling (including those already cold). Early attempts at forming spiral galaxies with cosmological, hydrodynamic simulations were plagued by an ‘angular-momentum catastrophe’, where gas cooled too quickly and lost too much angular momentum (see, e.g., Katz & Gunn 1991; Navarro & Benz 1991; Navarro & Steinmetz 1997, 2000). Solutions to this problem were found in better resolution (Governato et al. 2004) and more efficient subgrid feedback (e.g. Brook et al. 2011, 2012). We are now in a position to use a simulation like EAGLE to make predictions about angular-momentum conservation of cooling gas, or lack thereof, which is informative for analytic models of gas cooling.

We measure the specific angular momentum, j , of cooling and cooled particles (i.e. immediately before and after cooling) in our EAGLE haloes along their cooling axes on an individual basis and for the summed quantity of all cooling particles involved in a single episode. The relative change in j for each case is presented in the upper and middle panels of Fig. 9, respectively. We bin our systems by redshift, as in the previous sections, and show distributions for the relative change in angular momentum for each of these bins. Because resolution is known to play a role in j losses, we present both the Reference and RecalHR simulations in the left and right panels of Fig. 9, respectively.

It is clear from the top panels of Fig. 9 that individual particles do not conserve angular momentum while cooling. Comparing this to the middle panels, those particles appear

to be exchanging some of their angular momentum between one another, as the net change in j for the collection of particles provides a narrower distribution with a peak closer to zero. In both cases, the means of the distributions are negative. Therefore, on average, *angular momentum is lost by gas as it cools* onto EAGLE galaxies. There is no clear evolution in the distributions for either the upper or middle panels of Fig. 9. for the Reference simulation; for the highest- to lowest-redshift bins, the average net loss of j during a cooling episode is approximately 55, 64, and 57 per cent, respectively. The highest- and lowest-redshift histograms are also consistent according to the Kolmogorov–Smirnov test. We find that at higher resolution (the RecalHR run), j losses during cooling are reduced at higher redshift, on average. We suggest that, by itself, this is not enough to claim any generic correlation between $\Delta j/j_i$ and z , especially as the results between simulations agree at low redshift. We come back to this point in Section 4.2.

Galactic discs in EAGLE are known to be realistic in their size (Furlong et al. 2015b; Schaye et al. 2015; Lange et al. 2016). Yet, the gas that cools loses a fraction of angular momentum that is consistent with the large percentages reported when the ‘angular-momentum catastrophe’ produced simulated discs that were too concentrated (cf. Katz & Gunn 1991). While, indeed, too much *absolute* angular momentum was lost during cooling in early hydrodynamic, cosmological simulations, evidently the correct amount of *specific* angular momentum was lost, based on our results.

The frequency of particle interactions and collisions will determine the potential for angular-momentum loss of cooling particles. We hypothesise that in a rotationally supported system, where there is less random motion, collisions might be fewer, and thus less angular momentum might be lost. To test this, we first quantify the relative level of rotation and dispersion support in our galaxies using the λ_R parameter, introduced by Emsellem et al. (2007). Galaxies with $\lambda_R \sim 0$ are predominantly dispersion-supported,

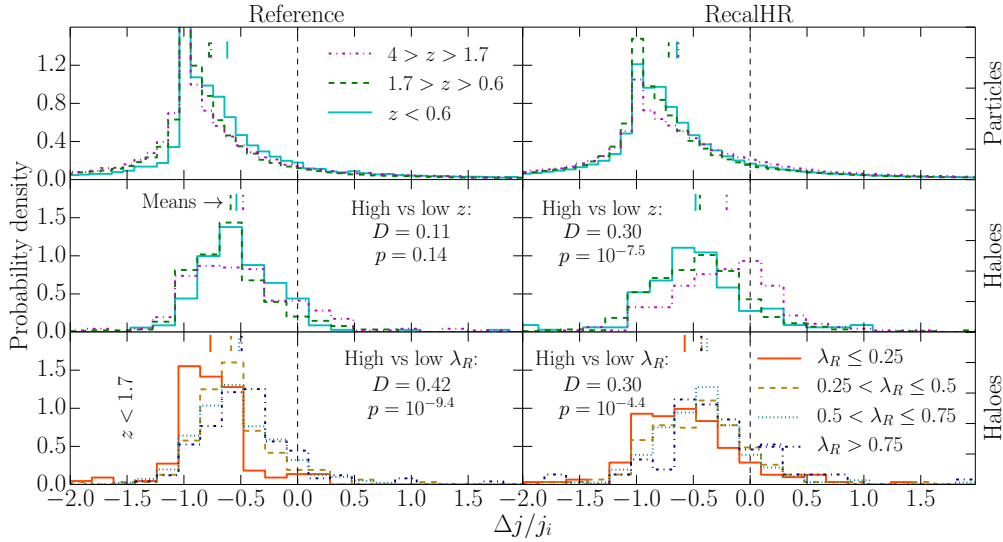


Figure 9: Relative change in the specific angular momentum component parallel to the rotation axis of cooling particles during cooling episodes, compared to the initial state. The left-hand panels include haloes from our Reference EAGLE sample, while the right-hand panels include those from the RecalHR run. The top panels consider particles individually. The middle and bottom panels consider the change in net specific angular momentum of all cooling particles in a single episode, i.e. on a halo-by-halo basis. Where the top two rows of panels bin by redshift, the bottom row of panels bins by the λ_R value of the central galaxy for all $z < 1.7$. The short vertical lines give the mean of each distribution for respective linestyle. If angular momentum were always conserved along the cooling axis, the distributions would be δ functions matching the long, vertical, dashed line. Instead, we see angular-momentum losses in the cooling gas. We perform Kolmogorov–Smirnov tests to compare the consistency of the halo distributions between $4 > z > 1.7$ and $z < 0.6$, and between the distributions for $\lambda_R \leq 0.25$ and $\lambda_R > 0.75$. The D -value printed in the panels gives the maximum vertical separation of the cumulative probability distributions, while the p -value is the probability that the means of the distributions would be as separated as they are under the pretext that they come from the same underlying population. A little less angular momentum appears to be lost when gas cools onto a rotationally supported galaxy.

whereas those with $\lambda_R \sim 1$ are predominantly rotationally supported. For our EAGLE galaxies, we measure the property as

$$\lambda_R = \frac{\sum_* m_* j_{z,*}}{\sum_* m_* \sqrt{j_{z,*}^2 + r_*^2 v_{z,*}^2}}, \quad (9)$$

where the sums are over all star particles associated with the main subhalo within the ‘BaryMP’ galactic radius defined by [Stevens et al. \(2014\)](#), where the cumulative mass profile of the stars and cold gas reaches a constant gradient), and j_z and v_z are the specific angular momentum and velocity components along the galaxy’s rotation axis, respectively, as measured in the galaxy’s centre-of-momentum frame.¹ In the bottom panels of Fig. 9, we again show the relative net loss of specific angular momentum during cooling events, but now bin galaxies by λ_R , including all systems for $z < 1.7$. By excluding those in the range $1.7 < z < 4$, we eliminate the population of high- z systems from RecalHR that we have shown lose less j during cooling. We would have otherwise had biased results, as the average λ_R of the galaxies is lower at higher z . For the Reference and RecalHR simulations, we find a weak, but statistically significant, tendency for j losses to be reduced for high- λ_R systems. The difference in the means is less for RecalHR than the Reference simulation,

but it is still in favour of our hypothesis. Our results suggest any reduction in j losses during cooling caused by stronger rotation in the central galaxy is, at most, a few tens of per cent.

4.2 Relative orientation and magnitude of specific angular momentum

As already discussed, galaxy formation models typically assume that the net specific angular momentum of hot gas about to cool, \vec{j}_{cooling} , is equivalent to that of all the hot gas in the halo, \vec{j}_{hot} , and to that of the entire halo itself, \vec{j}_{halo} , both in terms of magnitude and direction. Without the ability to directly measure the motion of dark matter in haloes to independently measure a halo’s spin, it is impossible to determine if \vec{j}_{cooling} and \vec{j}_{halo} are the same empirically with observational methods. Simulations are the only current means of addressing this in any capacity. Previous studies of cosmological, hydrodynamic simulations have shown that gas and dark matter in haloes tend to have different and offset specific angular momenta (e.g. [van den Bosch et al. 2002](#); [Chen, Jing & Yoshikawa 2003](#); [van den Bosch, Abel & Hernquist 2003](#); [Sharma & Steinmetz 2005](#); [Sharma, Steinmetz & Bland-Hawthorn 2012](#)). Attention has not been given specifically to the *cooling* particles before, however.

4.2.1 Magnitude

We directly measure the ratio $j_{\text{cooling}}/j_{\text{halo}}$ from our EAGLE haloes, and present distributions for this ratio for bins

¹ Note that this calculation for λ_R does not include the intricacies required to compare against observations as in [Naab et al. \(2014\)](#), as we simply require a relative measure of this quantity for internally comparing EAGLE galaxies.

of redshift in the top panels of Fig. 10. We see that cooling gas typically has more specific angular momentum than the halo. This result is contrasting (but not opposing) to the combined results of observations and models that suggest the stellar content of galaxies typically has lower specific angular momentum than their haloes (e.g. Romanowsky & Fall 2012; Stevens et al. 2016). As discussed in Section 4.1, some of this angular momentum is lost during the cooling process. As seen in the top panels of Fig. 10, there is no *clear* evolution in $j_{\text{cooling}}/j_{\text{halo}}$ for our EAGLE haloes. We do, however, find the mean ratio to be lower for RecalHR at higher redshift, which appears to be statistically significant, based on a Kolmogorov–Smirnov test (see the top right panel of Fig. 10). This is balanced by the fact that less angular momentum is lost during the cooling process for these specific haloes, as shown in Section 4.1. If we compare these findings with the lower left panel of Fig. 3, we see that the cooling gas in these haloes is lower at the ‘beginning’ of the cooling episode for the RecalHR run. The evidence suggests the population of RecalHR haloes in our sample for $4 > z > 1.7$ effectively had a head start in cooling over the same haloes in the Reference simulation, and thus were measured at a moment when the gas was already cooler and had already lost some of its specific angular momentum. This would imply the angular momentum measurements in the Reference and RecalHR runs are entirely consistent.

We have already shown tentative evidence that gas cooling onto a rotationally supported galaxy in EAGLE loses less specific angular momentum than that cooling onto a dispersion-supported galaxy (Fig. 9). In the bottom panels of Fig. 10 we also break $j_{\text{cooling}}/j_{\text{halo}}$ into bins of λ_R . There is a population of low- λ_R galaxies, in both the Reference and RecalHR simulations, that show high values for $j_{\text{cooling}}/j_{\text{halo}}$, but are not abnormal in any other respect we can find. We find nearly all the excess specific angular momentum is lost during cooling for these systems. Modulo those few systems, the distributions for $j_{\text{cooling}}/j_{\text{halo}}$ for various λ_R are entirely consistent with each other. In other words, gas should not be aware of what type of galaxy it will cool onto at the moment it begins to cool, which appears to indeed be the case for EAGLE.

4.2.2 Orientation

The direction of the angular momentum of the cooling gas is also important for how the new material will alter the disc. In the top panels of Fig. 11 we show the angular offsets of the spin vectors of hot gas about to cool and hot gas in general for our EAGLE haloes. Regardless of redshift, these are typically offset by tens of degrees. Interestingly, the particles about to cool show better alignment with the cold disc than with the hot gas from whence they came (cf. top and middle panels of Fig. 11). Because the cooling gas’s rotation axis is consistently offset from the hot gas a whole, an offset is built between the rotation axes of the cold gas in the galaxy and its hot halo; this is shown by the bottom panels of Fig. 11. Again, we find minimal difference between the Reference (left panels) and RecalHR (right panels) runs, suggesting this is indeed a physical effect.

Using the EAGLE simulations, Zavala et al. (2016) showed that the spin direction of a galaxy is more aligned with that of the inner parts of its halo ($< 0.1R_{\text{vir}}$) than that

of the entire halo. Also, because most cooling occurs in the inner part of the hot halo (Fig. 5), one might expect the inner hot halo’s rotation axis to be better aligned with the cooling gas. In light of these findings, we check whether the rotation axis offset between cooling and hot gas varies when only hot gas internal to a given radius is included. This is presented in Fig. 12. Contrary to expectation, the inner hot gas is typically *less* aligned with the cooling gas. Any evolution in these profiles is minimal for our sample of EAGLE haloes, as seen by the similarity of the curves in Fig. 12. The Reference (upper panel) and RecalHR (lower panel) simulations again produce the same result, so we can trust that this is not predominantly an effect of resolution.

The relative orientations and magnitudes of various particle types in haloes *in general* is an interesting topic which we are investigating in detail in an accompanying paper (Contreras et al. in preparation). The sample of cooling systems used here is consistent with the differences in direction and magnitude of j between baryons and dark matter in all EAGLE haloes to be presented there. That paper will address uncertainties in angular momentum as a function of the number of particles used; in general $\gtrsim 100$ particles is required for trustworthy measurements of individual haloes. We do not find any significant changes to our conclusions here (which are concerned with the *population*) if we exclude haloes with < 100 particles though.

5 AFTER COOLING: COLD GAS IN GALAXIES

5.1 Radial surface density profiles of gas discs

In the picture of disc formation proposed by Fall & Efstathiou (1980), gas cools and collapses to form an exponential disc while conserving angular momentum:

$$\Sigma_{\text{cooled}}(r) = \Sigma_0 e^{-r/r_d} \simeq \frac{m_{\text{cooled}}}{2\pi r_d^2} e^{-r/r_d}, \quad (10)$$

where $r_d \ll R_{\text{vir}}$ is the scale radius of the disc. The exponentiality of discs is a typical assumption of galaxy formation models, where some even maintain that a disc must always be exponential (e.g. Cole et al. 2000; Hatton et al. 2003; Croton et al. 2006, 2016; Somerville et al. 2008a; Guo et al. 2011). But only relatively recently have resolved observations of the H I and CO (H₂) distribution in local spiral galaxies been made (e.g. Walter et al. 2008; Leroy et al. 2009), allowing us to actually see what they are like. The 33 galaxies analysed by Bigiel & Blitz (2012) suggest that while an exponential profile broadly describes the average galaxy at intermediate radii, there is plenty of deviation from exponentials, and a strong suggestion of cusps existing at the centres of these discs. With EAGLE, we can not only check the exponentiality of gas discs, but also compare directly to equation (10).

We present surface density profiles for recently cooled and all cold gas of our sample of EAGLE haloes in Fig. 13 (top and bottom panels, respectively). To build these profiles, we find the rotation axis of the cold (cooled) particles to determine the plane of the galaxy (freshly cooled gas),

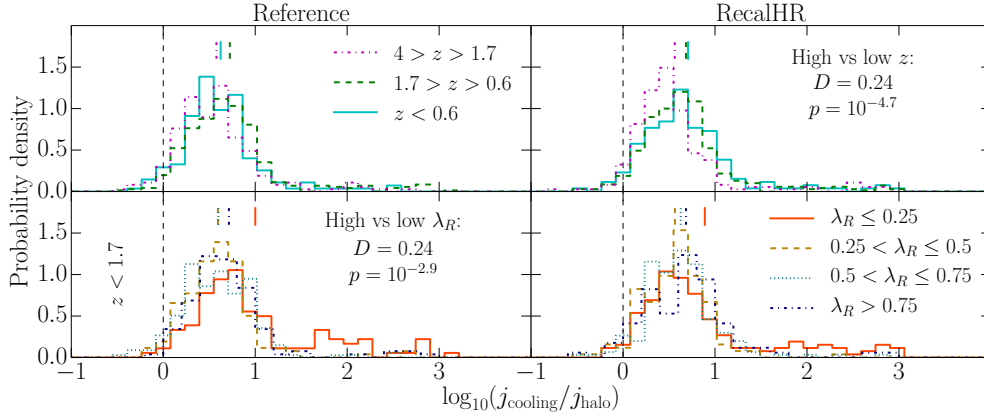


Figure 10: Probability distributions for the ratio of the magnitudes of net specific angular momentum of cooling gas to that of the halo, drawn from our sample of Reference and RecalHR EAGLE systems. The top panels cover all systems in each redshift bin, while the bottom panels cover all $z < 1.7$ and bins by λ_R of the central galaxy. The dashed, vertical line indicates where $j_{\text{cooling}} = j_{\text{halo}}$, which is often assumed in galaxy formation models. The short vertical lines mark the means of the distributions. We perform Kolmogorov–Smirnov tests on the consistency of the distributions in each panel, and note the cases where there is potential inconsistency (see caption of Fig. 9). Cooling gas carries more specific angular momentum than the halo on almost all occasions.

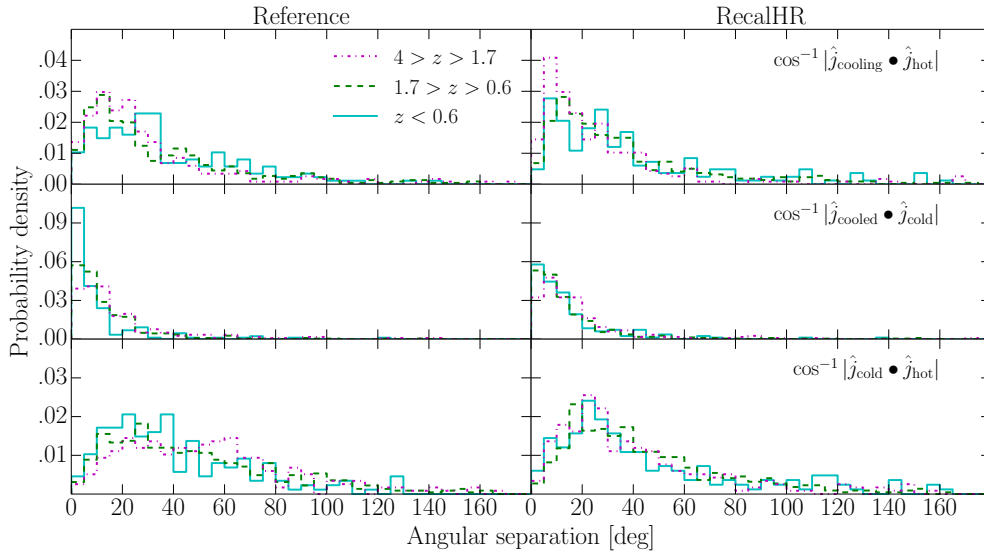


Figure 11: Angular separations between rotation axes of gas particle groups during cooling. The top panels give the difference between all the hot particles and those about to cool. The middle panels are for all cold gas and the particles that have just cooled. The bottom panels are for all cold gas and all hot gas. Gas that cools is better aligned with gas that is already cold than the rest of the hot gas in the halo.

and measure the surface density in annuli² in this plane. Consistent with our measurements of the hot gas profiles, the widths of the annuli are adapted to contain the same number of particles, while respecting the softening scale. 100 annuli are used for the cold gas, 20 for the cooled gas. We then fit an exponential to each profile and normalise the annuli’s radii by the fitted scale length. By normalising the surface densities as well, we are able to see how well an exponential describes the entire galaxy population as a whole. Note that $r_{\text{d,fit}}$ is a different quantity for the the $\Sigma_{\text{cooled}}(r)$ and $\Sigma_{\text{cold}}(r)$ profiles in Fig. 13.

² For our intents and purposes, an annulus is a cylindrical shell that cannot exceed the virial sphere in height.

The top panels of Fig. 13 show that $\Sigma_{\text{cooled}}(r)$ for EAGLE galaxies is nicely centred on equation (10), with a scatter increasing at lower redshift (the 68% confidence range is 0.53, 0.62, and 0.79 dex tall on average for the highest-to lowest-redshift bins, respectively). The profiles include a cusp, seen at $r \lesssim 0.6r_a$ for the highest-redshift bin, with the prominence of this feature growing modestly down to $z = 0$.

Of course, the galaxies in our sample need not be all rotationally supported, and hence may not have well-behaving, classical discs. To this point, we over-plot the median surface density profiles for cold and recently cooled gas for the rotation-dominated galaxies with $\lambda_R > 0.75$ in Fig. 13 with dot-dashed curves. By selecting galaxies we expect to be more disc-like, we find no difference in the normalised surface density profiles for cold or recently cooled gas. While

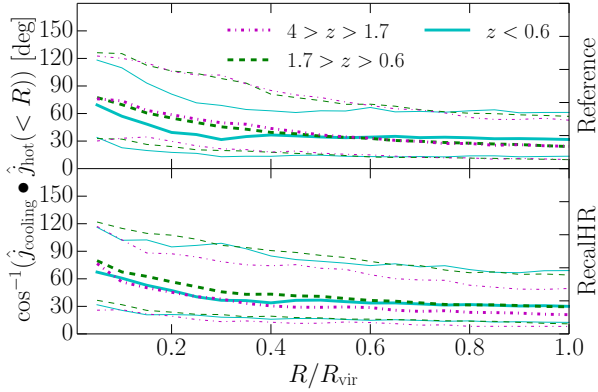


Figure 12: Angular separation between spin directions of hot gas in haloes within a given radius and all cooling gas within in the same haloes. Cooling gas is poorly aligned with hot gas on all scales, regardless of redshift or resolution.

the recently cooled gas in these galaxies lost less j during the cooling process, this has not translated into a difference in $\Sigma_{\text{cooled}}(r)$.

In a semi-analytic model, one must put in what the scale length of the cooling disc is. Fall (1983) and Mo et al. (1998) have shown that by assuming the gas cools from a singular isothermal sphere, that $j_{\text{halo}} = j_{\text{cooling}} = j_{\text{cooled}}$, and the rotation curve of this gas is completely flat, where $v_{\text{rot}} = V_{\text{vir}}$, the scale radius can be related to the spin of the halo:

$$r_{\text{d,model}} \equiv \frac{\lambda}{\sqrt{2}} R_{\text{vir}} = \frac{j_{\text{halo}}}{2V_{\text{vir}}}, \quad (11)$$

where λ is the dimensionless spin parameter (Peebles 1969; Bullock et al. 2001):

$$\lambda \equiv \frac{J|E|^{1/2}}{GM_{\text{vir}}^{5/2}} = \frac{j_{\text{halo}}}{\sqrt{2}V_{\text{vir}}R_{\text{vir}}} \quad (12)$$

(with J and E the total angular momentum and energy of the halo, respectively). This model also assumes λ measured from a dark-matter-only simulation is equivalent to considering all matter in a halo in reality (which might not be true – Schaller et al. 2015a, for example, have shown the masses of haloes in the EAGLE simulations are systematically higher when run without baryonic physics). Equation (11) has formed the basis of determining (initial) disc sizes in many semi-analytic models (e.g. Hatton et al. 2003; Croton et al. 2006; Fu et al. 2010), but more complex algorithms are also popular (e.g. Cole et al. 2000). We showed in Section 4 that the assumptions about the angular momentum of the cooling gas required for equation (11) to be accurate do not agree with EAGLE, so we would expect some difference between the model scale length, $r_{\text{d,model}}$, and the fitted scale length, $r_{\text{d,fit}}$. After measuring net specific angular momentum of each halo in our EAGLE sample as

$$j_{\text{halo}} = \frac{|\sum_p m_p \vec{r}_p \times \vec{v}_p|}{\sum_p m_p} \quad (13)$$

(where subscript p is for particles of all types within R_{vir}), we can quantify how discrepant $r_{\text{d,model}}$ is from $r_{\text{d,fit}}$.

In Fig. 14(a), we present normalised histograms for the ratio of $r_{\text{d,fit}}/r_{\text{d,model}}$ for both the Reference and RecalHR

haloes, for all $z < 4$. Both simulations find an almost log-normal distribution for this ratio, where it is almost always true that $r_{\text{d,fit}} > r_{\text{d,model}}$. The idea that $r_{\text{d}} \propto j_{\text{halo}}/V_{\text{vir}}$ (equation 11) came from the assumptions that $j_{\text{cooled}} = j_{\text{halo}}$ and that the cooled gas all rotated with velocity V_{vir} . In practice, we should really expect $r_{\text{d}} \propto j_{\text{cooled}}/v_{\text{rot}}$, where v_{rot} is mass-weighted mean tangential velocity of the cooled gas. This then gives

$$\frac{r_{\text{d,fit}}}{r_{\text{d,model}}} \simeq \frac{j_{\text{cooled}} V_{\text{vir}}}{j_{\text{halo}} v_{\text{rot}}}. \quad (14)$$

In Fig. 14(b), we compare the left- and right-hand side of equation (14) for the Reference and RecalHR simulation haloes, displaying the median and 16th–84th percentile range for each. Note that we have binned data along the y -axis of this plot (and Fig. 14d, but all other plots in this paper bin along the x -axis). Both simulations corroborate equation (14), with the median trend for the RecalHR simulation (with ≥ 512 cooled particles per halo) nearly matching it perfectly. In addition to an exponential not describing *every individual* cooling profile, the scatter in Fig. 14(b) can be attributed to the cooling particles having an angular-momentum structure (see Section 5.2) where the specific angular momentum of individual particles does not have a precise monotonic relationship with either position or rotational velocity.

It is useful to relate $r_{\text{d,fit}}/r_{\text{d,model}}$ to global properties of the halo, as, if there is a strong correlation with one, the prescription for calculating r_{d} in a semi-analytic model could be easily modified to better match the results of EAGLE. We find that the halo property that best correlates with $r_{\text{d,fit}}/r_{\text{d,model}}$ is the spin parameter, λ . This is shown in Fig. 14(d). By performing a least-squares fit for $\log_{10}(r_{\text{d,fit}}/r_{\text{d,model}})$ as a function of $\log_{10} \lambda$ for the RecalHR simulation, we obtain the relation

$$\log_{10} \left(\frac{r_{\text{d,fit}}}{r_{\text{d,model}}} \right) = -0.77 \log_{10} \lambda - (0.52 \pm 0.18), \quad (15)$$

where the uncertainty is the standard deviation of the points about the fit. Combining this result and equation (11), we suggest a modified model for the scale radius of cooling gas in a halo of given size and spin:

$$\log_{10} \left(\frac{r_{\text{d}}}{R_{\text{vir}}} \right) = 0.23 \log_{10} \lambda - 0.67 (\pm 0.18). \quad (16)$$

In Fig. 14(e), we show that our EAGLE haloes are representative in terms of their distribution of spins, which should be roughly log-normal (cf. Barnes & Efstathiou 1987; Bullock et al. 2001).

5.2 Angular-momentum structure of gas discs

There is a building trend for models of disc evolution to calculate local processes in annuli of specific angular momentum, rather than radius (e.g. Stringer & Benson 2007; Dutton & van den Bosch 2009; Stevens et al. 2016). These have been partially motivated by the fact that galaxies have dynamic and non-uniform velocity structures. One can rewrite equation (11) as an exponential function of specific angular momentum, thereby relaxing the requirement that cooling gas should settle with a constant rotational velocity:

$$\Sigma_{\text{cooled}}(j) = \Sigma_0(j_{\text{d}}) e^{-j/j_{\text{d}}} \quad (17)$$

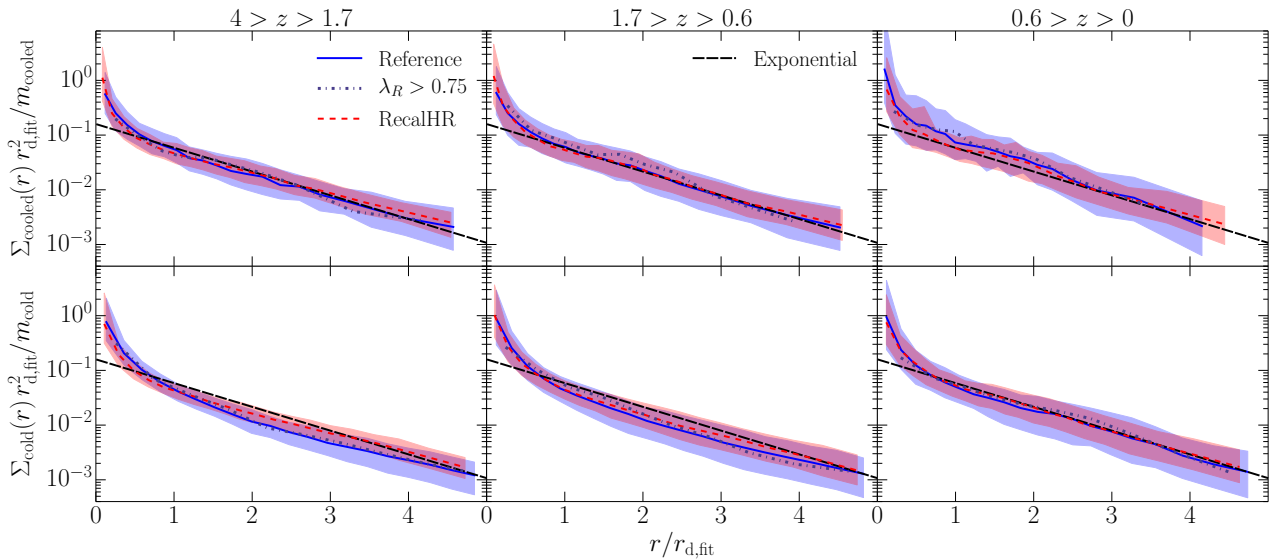


Figure 13: Surface density profiles for cold gas particles in our sample of EAGLE galaxies. As for previous figures, we present 3 redshift ranges for the Reference and RecalHR simulations, presenting their median profiles (solid and short-dashed curves, respectively) and 16th–84th percentile ranges (shaded regions). Radial distances have been normalised for each galaxy by their fitted exponential scale radius, $r_{d,fit}$. The top row of panels considers only the recently cooled particles, whereas the bottom panels consider all cold particles. All surface densities have been normalised by the amount of cooled/cold gas considered and the square of the scale radius. The long-dashed line is a precise exponential (equation 10). The dot-dashed curves give the median profile for the rotation-dominated galaxies ($\lambda_R > 0.75$) for each subsample of the Reference haloes. With the addition of a central cusp, an exponential describes the profile of recently cooled gas well, but only works as well for cold discs as a whole at low redshift.

(e.g. as implemented in the DARK SAGE semi-analytic model; Stevens et al. 2016). Here, we investigate the angular-momentum structure of the cooled and cold gas profiles of our EAGLE galaxies and determine whether equation (17) can approximate them.

We measure the mean j of particles in each annulus for which we have measured surface density values for our EAGLE galaxies. This gives us $\Sigma_{cooled}(j)$ and $\Sigma_{cold}(j)$ profiles, to which we fit equation (17), then normalise these profiles based on the fitted j_d . These are presented in Fig. 15. At intermediate to low redshifts, an exponential for $\Sigma_{cooled}(j)$ describes the profiles reasonably well, but this is not the case at high redshift. For $1.7 > z > 0.6$, there is less of a featured cusp for $\Sigma_{cooled}(j)$ than for $\Sigma_{cooled}(r)$. This could be explained by the rotational velocities (and hence specific angular momenta) decreasing rapidly at the centres of discs, where pressure support becomes comparable to rotational support. In general, we find the scatter in the profiles is reduced when considering surface density as a function of radius instead (cf. Figs 13 and 15). We find these conclusions extend to the overall cold gas profile, and that they apply to the general galaxy population (in our sample) as well as the most rotationally supported systems ($\lambda_R > 0.75$, which should be the most discy – cf. solid and dot-dashed curves in Fig. 15).

While our findings suggest one would be better off using equation (10) rather than (17) in a model of galaxy formation, it has been shown that using this expression for cooling in a semi-analytic model with disc structure can successfully reproduce the properties of local galaxies, including the relation between total mass and specific angular momentum of stellar discs (Stevens et al. 2016). Of course, disc instabilities and feedback will regulate the structure of a galaxy (both

as a function of specific angular momentum and radius), so the manner in which gas cools does not provide a complete picture by itself. An assessment of the importance of details surrounding cooling versus internal regulatory processes in accurately describing galaxy evolution with respect to observations would serve as a useful follow-up study to this work.

6 SUMMARY

We have studied the hot mode of accretion of gas onto galaxies in the EAGLE simulations. As detailed in Section 2.3, we selected systems where a sufficient number of gas particles cooled between snapshots in order to learn about the state of haloes undergoing cooling and the galaxies they host. Our findings presented in this paper can be summarised as follows.

- The temperature of hot gas in haloes is within a factor of 2 of the virial temperature across all radii (Section 3.1). The gradient of the temperature profiles steepens with time, due in part to stellar feedback. As centres become hotter, they become less dense, leading to shallower density gradients and the formation of a core in the hot gas (Section 3.2). The hot-gas density profiles are well approximated by a β profile, which can be parametrized as a simple function of redshift (equation 6).
- Using the precise density, temperature, and metallicity profiles of hot gas in the EAGLE haloes leads to range of cooling radii that is wider than one would obtain assuming a singular isothermal sphere or β profile for a halo with the same total mass content, net metallicity, and virial temperature. At low redshift, these cooling radii are systematically

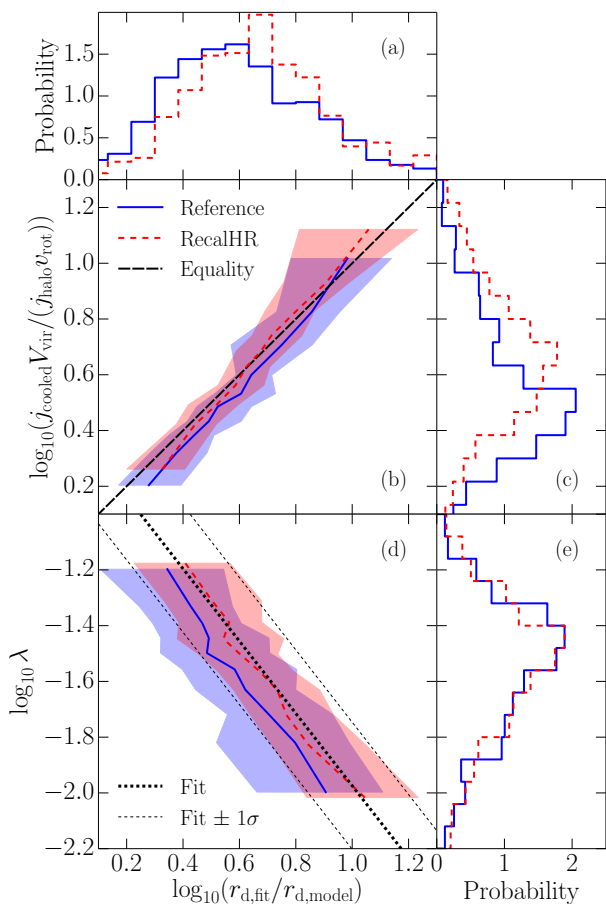


Figure 14: Trends relating to the ratio of the fitted exponential scale length of the surface density profiles of recently cooled gas in EAGLE galaxies to a typical assumed scale length in semi-analytic models (equation 11). *Panel (a):* Normalised histograms for this ratio for each of the Reference and RecalHR simulations. *Panel (b):* Relation between this ratio and a combination of the specific angular momentum of the cooled gas, that of the halo, the virial velocity of the halo, and the rotational velocity of the cooled gas. These quantities are expected to be nearly equal (equation 14, as given by the long-dashed line). The solid and short-dashed curves give the median for the Reference and RecalHR simulations respectively, with the 16th–84th percentile range for each shown by the shaded regions (for data binned along the y -axis). *Panel (c):* Normalised histograms for the y -axis value of panel (b). *Panel (d):* Relation between the scale radius ratio and the spin parameter of the halo. In addition to the median and 16th–84th percentile range (for data binned along the y -axis), we include a least-squares fit for the RecalHR simulation, including the standard deviation for points about this fit, where $\log_{10} \lambda$ has been taken as the independent variable. *Panel (e):* Normalised histograms for the spin parameter of the haloes. Only in the highest-spin haloes do the specific angular momenta of the cooled gas and halo become similar enough for the scale radius to resemble the model value.

smaller as well, which would translate into lower cooling rates under the model of White & Frenk (1991).

- The temperature and density profiles of cooling gas remain nearly unchanged with time, irrespective of the underlying hot gas (Section 3.1). Outflows from AGN feedback appear to help regulate the former. While perhaps most alike an exponential, the density profiles of cooling gas are consis-

tent with a singular isothermal sphere (Section 3.2). So long as models only require cooling gas to look like it is coming from an isothermal sphere, this seems to be a reasonable approximation.

- Over the course of cooling, gas loses approximately 60% of its specific angular momentum, on average (Section 4.1). This value is comparable to losses quoted during reports of the ‘angular momentum catastrophe’, yet the galaxies in EAGLE are far from catastrophic. We find a weak tendency for gas cooling onto rotationally supported galaxies to lose a lesser fraction of its specific angular momentum.

- Gas in the process of cooling typically begins with specific angular momentum several times greater than that of the halo and is offset from the rest of the hot gas by tens of degrees (Section 4.2). Despite this, freshly cooled gas is typically well aligned with pre-existing gas discs. Interestingly, the inner hot gas of the halo is even less well aligned with the cooling gas, despite the cooling gas predominantly originating from the inner halo (cf. Sections 3.2 and 4.2).

- Recently cooled gas is well approximated by an exponential surface density profile as a function of radius (Section 5.1). In general, this is more precise than an exponential as a function of specific angular momentum (Section 5.2). Because the cooled gas tends to have higher specific angular momentum than that of the halo, the best-fitting scale radius for these surface density profiles is typically larger than expected from the standard model of disc formation (Fall & Efstathiou 1980; Mo et al. 1998). This radius is still strongly tied to the spin parameter of a halo, for which we provide a new expression (equation 16).

Our results suggest some of the assumptions surrounding cooling of hot gas in (semi-)analytic galaxy formation models should be revised. While the parameters of models are often tuned to match the properties of galaxies in the local Universe, by altering the prescriptions surrounding cooling, the star formation histories and higher-redshift properties of these galaxies will change. This could, therefore, be fruitful in the quest for developing a model of galaxy evolution that can simultaneously explain the high- and low-redshift Universe.

ACKNOWLEDGEMENTS

We thank the city of Perth for its record heat-wave inspiring the title of this paper.

This work was supported by a Research Collaboration Award at the University of Western Australia. Parts of this research were conducted by the Australian Research Council Centre of Excellence for All-sky Astrophysics (CAASTRO), through project number CE110001020. SC acknowledges support from CONICYT Doctoral Fellowship Programme.

We acknowledge the Virgo Consortium for making their simulation data available. We thank PRACE for the access to the Curie facility in France. We have used the DiRAC system which is a part of National E-Infrastructure at Durham University, operated by the Institute for Computational Cosmology on behalf of the STFC DiRAC HPC Facility (www.dirac.ac.uk); the equipment was funded by BIS National E-infrastructure capital grant ST/K00042X/1,

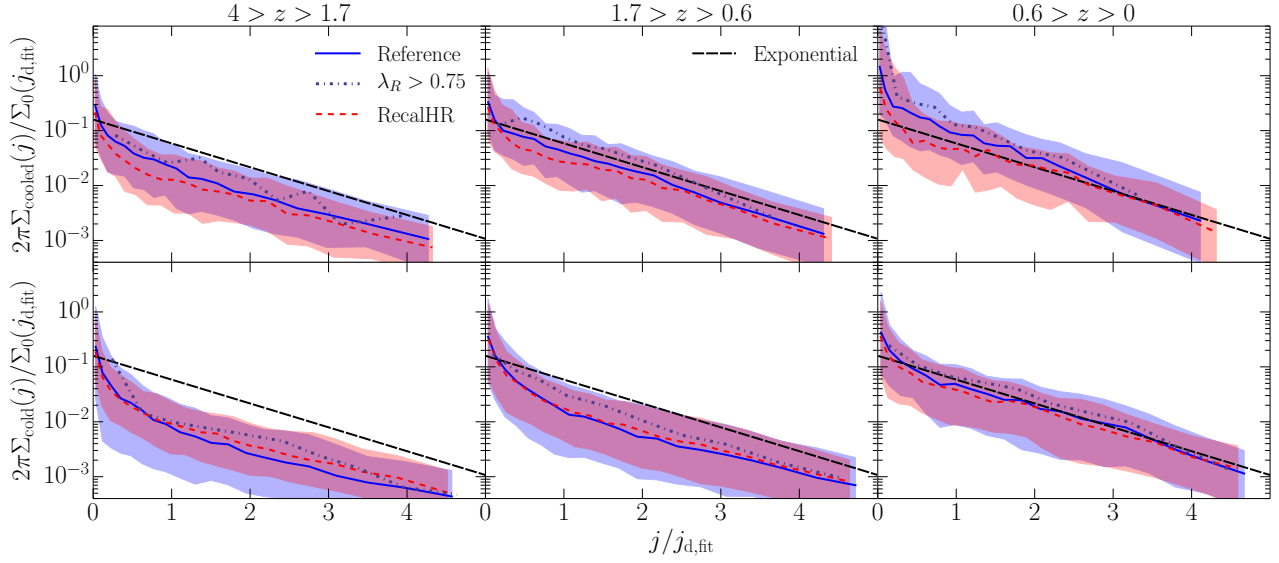


Figure 15: As for Fig. 13, but now presenting normalised surface density profiles for recently cooled (top panels) and all cold (bottom panels) gas as a function of specific angular momentum. If these profiles were generally well described by an exponential, we should see a tight relation about the long-dashed line in each panel. Instead, we find an exponential as a function of specific angular momentum is a less accurate description of the profiles to one as a function of radius (cf. Fig. 13).

STFC capital grant ST/H008519/1, STFC DiRAC Operations grant ST/K003267/1 and Durham University. The study was sponsored by the Dutch National Computing Facilities Foundation (NCF) for the use of supercomputer facilities, with financial support from the Netherlands Organisation for Scientific Research (NWO), and the European Research Council under the European Union’s Seventh Framework Programme (FP7/2007- 2013) / ERC Grant agreement 278594-GasAroundGalaxies.

REFERENCES

- Bahé Y. M. et al., 2016, *MNRAS*, 456, 1115
 Baldry I. K. et al., 2012, *MNRAS*, 421, 621
 Barnes J., Efstathiou G., 1987, *ApJ*, 319, 575
 Benson A. J., 2012, *NewA*, 17, 175
 Benson A. J., Bower R., 2011, *MNRAS*, 410, 2653
 Benson A. J., Pearce F. R., Frenk C. S., Baugh C. M., Jenkins A., 2001, *MNRAS*, 320, 261
 Benson A. J., Bower R. G., Frenk C. S., Lacey C. G., Baugh C. M., Cole S., 2003, *ApJ*, 599, 38
 Bertschinger E., 1989, *ApJ*, 340, 666
 Bigiel F., Blitz L., 2012, *ApJ*, 756, 183
 Birnboim Y., Dekel A., 2003, *MNRAS*, 345, 349
 Bondi H., 1952, *MNRAS*, 112, 195
 Bower R. G., Benson A. J., Malbon R., Helly J. C., Frenk C. S., Baugh C. M., Cole S., Lacey C. G., 2006, *MNRAS*, 370, 645
 Brook C. B. et al., 2011, *MNRAS*, 415, 1051
 Brook C. B., Stinson G., Gibson B. K., Roškar R., Wadsley J., Quinn T., 2012, *MNRAS*, 419, 771
 Bullock J. S., Dekel A., Kolatt T. S., Kravtsov A. V., Klypin A. A., Porciani C., Primack J. R., 2001, *ApJ*, 555, 240
 Cattaneo A. et al., 2007, *MNRAS*, 377, 63
 Chabrier G., 2003, *PASP*, 115, 763
 Chen D. N., Jing Y. P., Yoshikawa K., 2003, *ApJ*, 597, 35
 Cole S., Lacey C. G., Baugh C. M., Frenk C. S., 2000, *MNRAS*, 319, 168
 Cora S. A., 2006, *MNRAS*, 368, 1540
 Crain R. A. et al., 2015, *MNRAS*, 450, 1937
 Croton D. J. et al., 2006, *MNRAS*, 365, 11
 Croton D. J. et al., 2016, *ApJS*, 222, 22
 Dalla Vecchia C., Schaye J., 2012, *MNRAS*, 426, 140
 Dolag K., Borgani S., Murante G., Springel V., 2009, *MNRAS*, 399, 497
 Dubois Y., Devriendt J., Slyz A., Teyssier R., 2012, *MNRAS*, 420, 2662
 Durier F., Dalla Vecchia C., 2012, *MNRAS*, 419, 465
 Dutton A. A., van den Bosch F. C., 2009, *MNRAS*, 396, 141
 Emsellem E. et al., 2007, *MNRAS*, 379, 401
 Fall S. M., 1983, in Athanassoula E., ed., *Proc. IAU Symp.* 100, Internal Kinematics and Dynamics of Galaxies, Dordrecht, p. 391
 Fall S. M., Efstathiou G., 1980, *MNRAS*, 193, 189
 Font A. S. et al., 2008, *MNRAS*, 389, 1619
 Fu J., Guo Q., Kauffmann G., Krumholz M. R., 2010, *MNRAS*, 409, 515
 Furlong M. et al., 2015a, *MNRAS*, 450, 4486
 Furlong M. et al., 2015b, preprint (arXiv:1510.05645)
 Gonzalez-Perez V., Lacey C. G., Baugh C. M., Lagos C. D. P., Helly J., Campbell D. J. R., Mitchell P. D., 2014, *MNRAS*, 439, 264
 Governato F. et al., 2004, *ApJ*, 607, 688
 Guo Q. et al., 2011, *MNRAS*, 413, 101
 Guo Q. et al., 2016, *MNRAS*, 461, 3457
 Haardt F., Madau P., 2001, in Neumann D. M., Tran J. T. V., eds, *Clusters of Galaxies and the High Redshift Universe Observed in X-rays*
 Hatton S., Devriendt J. E. G., Ninin S., Bouchet F. R., Guiderdoni B., Vibert D., 2003, *MNRAS*, 343, 75
 Helly J. C. et al., 2003, *MNRAS*, 338, 913
 Henriques B. M. B., White S. D. M., Thomas P. A., Angulo R., Guo Q., Lemson G., Springel V., Overzier R., 2015, *MNRAS*, 451, 2663
 Katz N., Gunn J. E., 1991, *ApJ*, 377, 365
 Kauffmann G., White S. D. M., Guiderdoni B., 1993, *MNRAS*, 264, 201
 Kauffmann G., Colberg J. M., Diaferio A., White S. D. M., 1999, *MNRAS*, 303, 188

Kennicutt Jr. R. C., 1998, *ApJ*, 498, 541
Kereš D., Katz N., Weinberg D. H., Davé R., 2005, *MNRAS*, 363, 2
Lacey C. G. et al., 2015, preprint (arXiv:1509.08473)
Lagos C. d. P., Cora S. A., Padilla N. D., 2008, *MNRAS*, 388, 587
Lagos C. d. P., Padilla N. D., Davis T. A., Lacey C. G., Baugh C. M., Gonzalez-Perez V., Zwaan M. A., Contreras S., 2015a, *MNRAS*, 448, 1271
Lagos C. d. P. et al., 2015b, *MNRAS*, 452, 3815
Lagos C. d. P., Theuns T., Stevens A. R. H., Cortese L., Padilla N. D., Davis T. A., Contreras S., Croton D., 2016, *MNRAS* submitted
Lange R. et al., 2016, preprint (arXiv:1607.01096)
Lee J., Yi S. K., 2013, *ApJ*, 766, 38
Leroy A. K. et al., 2009, *AJ*, 137, 4670
Li C., White S. D. M., 2009, *MNRAS*, 398, 2177
Lu Y., Kereš D., Katz N., Mo H. J., Fardal M., Weinberg M. D., 2011, *MNRAS*, 416, 660
McConnell N. J., Ma C.-P., 2013, *ApJ*, 764, 184
Mo H. J., Mao S., White S. D. M., 1998, *MNRAS*, 295, 319
Monaco P., Fontanot F., Taffoni G., 2007, *MNRAS*, 375, 1189
Mulchaey J. S., 2000, *ARA&A*, 38, 289
Naab T. et al., 2014, *MNRAS*, 444, 3357
Navarro J. F., Benz W., 1991, *ApJ*, 380, 320
Navarro J. F., Steinmetz M., 1997, *ApJ*, 478, 13
Navarro J. F., Steinmetz M., 2000, *ApJ*, 538, 477
Padilla N. D., Salazar-Albornoz S., Contreras S., Cora S. A., Ruiz A. N., 2014, *MNRAS*, 443, 2801
Peebles P. J. E., 1969, *ApJ*, 155, 393
Planck Collaboration XVI, 2014, *A&A*, 571, A16
Romanowsky A. J., Fall S. M., 2012, *ApJS*, 203, 17
Rosas-Guevara Y. M. et al., 2015, *MNRAS*, 454, 1038
Saro A., De Lucia G., Borgani S., Dolag K., 2010, *MNRAS*, 406, 729
Schaller M. et al., 2015a, *MNRAS*, 451, 1247
Schaller M., Dalla Vecchia C., Schaye J., Bower R. G., Theuns T., Crain R. A., Furlong M., McCarthy I. G., 2015b, *MNRAS*, 454, 2277
Schaye J., 2004, *ApJ*, 609, 667
Schaye J., Dalla Vecchia C., 2008, *MNRAS*, 383, 1210
Schaye J. et al., 2015, *MNRAS*, 446, 521
Sharma S., Steinmetz M., 2005, *ApJ*, 628, 21
Sharma S., Steinmetz M., Bland-Hawthorn J., 2012, *ApJ*, 750, 107
Shen S., Mo H. J., White S. D. M., Blanton M. R., Kauffmann G., Voges W., Brinkmann J., Csabai I., 2003, *MNRAS*, 343, 978
Somerville R. S. et al., 2008a, *ApJ*, 672, 776
Somerville R. S., Hopkins P. F., Cox T. J., Robertson B. E., Hernquist L., 2008b, *MNRAS*, 391, 481
Springel V., 2005, *MNRAS*, 364, 1105
Springel V., White S. D. M., Tormen G., Kauffmann G., 2001, *MNRAS*, 328, 726
Springel V., Di Matteo T., Hernquist L., 2005, *MNRAS*, 361, 776
Stevens A. R. H., Martig M., Croton D. J., Feng Y., 2014, *MNRAS*, 445, 239
Stevens A. R. H., Croton D. J., Mutch S. J., 2016, *MNRAS*, 461, 859
Stringer M. J., Benson A. J., 2007, *MNRAS*, 382, 641
Sutherland R. S., Dopita M. A., 1993, *ApJS*, 88, 253
Tonini C., Mutch S. J., Croton D. J., Wyithe J. S. B., 2016, *MNRAS*, 459, 4109
van den Bosch F. C., Abel T., Croft R. A. C., Hernquist L., White S. D. M., 2002, *ApJ*, 576, 21
van den Bosch F. C., Abel T., Hernquist L., 2003, *MNRAS*, 346, 177
Viola M., Monaco P., Borgani S., Murante G., Tornatore L., 2008, *MNRAS*, 383, 777

Walter F., Brinks E., de Blok W. J. G., Bigiel F., Kennicutt Jr. R. C., Thornley M. D., Leroy A., 2008, *AJ*, 136, 2563
White S. D. M., Frenk C. S., 1991, *ApJ*, 379, 52
White S. D. M., Rees M. J., 1978, *MNRAS*, 183, 341
Wiersma R. P. C., Schaye J., Smith B. D., 2009a, *MNRAS*, 393, 99
Wiersma R. P. C., Schaye J., Theuns T., Dalla Vecchia C., Tornatore L., 2009b, *MNRAS*, 399, 574
Yoshida N., Stoehr F., Springel V., White S. D. M., 2002, *MNRAS*, 335, 762
Zavala J. et al., 2016, *MNRAS*, 460, 4466

APPENDIX A: MODEL-EQUIVALENT COOLING RATES

In an ideal world, one would know the unique density, temperature, and metallicity profile of hot gas in every halo processed through a semi-analytic model. By using the measured profiles from EAGLE, we can solve equation (8) numerically for each halo, thereby determining the ‘semi-analytic equivalent’ for the cooling rate with ideal information. This can be compared against a more realistic calculation for a semi-analytic model, where in addition to an analytic density profile, it is assumed that $T_{\text{hot}}(R) = T_{\text{vir}}$ and $Z_{\text{hot}}(R) = Z_{\text{hot}}$ for each halo. The results of Section 3.4 suggest any of a singular isothermal sphere, a β profile with $c_\beta = 0.1$, or a β profile with $c_\beta(z)$ from equation (6) will work practically the same for calculating a cooling rate. In the left-hand panel of Fig. A1 we compare the cooling rates calculated by equation (7) using the full EAGLE profile information against the case of an assumed singular isothermal sphere (we have checked that this is essentially the same for the case of a β profile).

The spread in the true R_{cool} values for the EAGLE haloes is greater than that of the analytic models, as seen in all panels of Fig. 8. This then gives rise to the notable spread in the relative cooling rates seen in the left-hand (and middle, see below) panel of Fig. A1. In the lower redshift bins, the model R_{cool} values are systematically too large, most clearly seen in the right-hand panel of Fig. 8. This then translates into systematically higher cooling rates, as seen by the evolution in the distributions of the left-hand (and middle) panel of Fig. A1.

Note that the cooling rates calculated by equation (8) do not consider feedback (of any kind), and hence are *gross* cooling rates (as opposed to *net* cooling rates – see below). If feedback were to affect the density or temperature profiles of the hot gas in haloes significantly, then we might expect this feedback to still cause differences in the gross cooling rates. While we showed that feedback does alter the temperature at the centre of EAGLE haloes in Fig. 4, this is less than a factor of 2. Because the hot-gas density profiles also do not change significantly when the strength of feedback is varied, the gross cooling rates calculated by equation (8) should agree for the Reference and alternate-feedback simulations. To demonstrate one example, we compare \dot{m}_{cool} for the NoAGN simulation, as we did for the Reference simulation, in the middle panel of Fig. A1. While there are small differences compared with the left-hand panel, the evolution of the distributions and their peaks are in agreement. Results for WeakFB and StrongFB are indeed similar, so we omit them for simplicity.

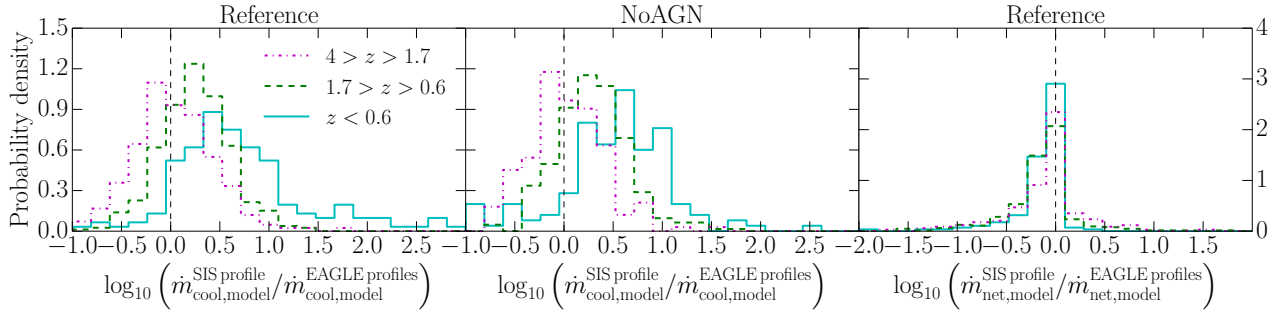


Figure A1: Normalised histograms for the relative analytic cooling rates calculated for model density profiles of hot gas versus those using the actual density, temperature, and metallicity profiles from our sample of Reference and NoAGN EAGLE haloes, as labelled. The left and middle panels compare gross cooling rates (equation 8), while the right-hand panel compares net cooling rates (equation A2). If the analytic approximations were sufficient for calculating cooling rates, the distributions would be δ functions at the vertical dashed line.

While stellar feedback is often considered independently of calculating cooling rates in semi-analytic models (but not always – see, e.g., Monaco et al. 2007), radio mode AGN feedback is generally implemented by *directly* suppressing the cooling rates calculated through equation (8) (see Bower et al. 2006; Croton et al. 2006). Galaxies hosting a larger supermassive black hole will typically have their cooling suppressed more. At later times, the haloes in our sample are bigger (see Fig. 2) and host heavier black holes. Because the suppressive heating from AGN need not be tied directly to the gross cooling rates of haloes, ratios of *net* cooling rates as calculated in semi-analytic models with different hot-gas radial profiles will not be the same as the ratio of *gross* cooling rates. They will, in fact, be systematically smaller for systems with an AGN, effectively counteracting the redshift evolution of the gross cooling rate ratios presented in the left (and central) panels of Fig A1.

To demonstrate the impact AGN heating might have on cooling rates in semi-analytic model, we use an example model of AGN heating to calculate effective net cooling rates for the haloes. We calculate the heating rate based on energy released from Bondi–Hoyle accretion (Bondi 1952) of hot gas in the halo

$$\dot{m}_{\text{heat,model}} = \frac{15\pi}{16} \frac{(\bar{\mu}m_p)^2}{\Lambda(T_{\text{vir}}, \bar{Z}_{\text{hot}})} Gc^2 \kappa \eta m_{\text{BH}} \quad (\text{A1})$$

(as implemented similarly in Croton et al. 2006; Somerville et al. 2008b), where m_{BH} is the black-hole mass,³ κ is a model parameter used to control the strength of feedback, and η is the efficiency with which the inertial mass of particles is released during accretion onto the black hole. Here, we assume typical values of $\kappa = \eta = 0.1$. The net cooling rate of gas in a halo can then be found as the difference between equations (8) and (A1):

$$\dot{m}_{\text{net,model}} = \dot{m}_{\text{cool,model}} - \dot{m}_{\text{heat,model}} \quad (\text{A2})$$

We calculate \dot{m}_{net} for our haloes in the Reference simulation, using the true and analytic (singular isothermal sphere

and β) radial profiles. In the right-hand panel of Fig. A1 we present the ratio of the model-equivalent net cooling rates using the EAGLE radial profiles (density, temperature, and metallicity) to the singular isothermal sphere profile. Not only is the evolution of the distributions minimised compared to the ratio of gross cooling rates, but the widths of the distributions are also greatly reduced. The latter would not be true if the central temperature and metallicity of the hot haloes were used in the Bondi–Hoyle model, however.

³ 94% of the (sub)haloes in our sample have more than one black-hole particle. In a semi-analytic model, galaxies typically are only allowed one black hole; when a merger brings in a new black hole, it is assumed to merge immediately with any pre-existing black hole. To mimic this, we sum the masses of all black holes in an EAGLE galaxy to calculate $\dot{m}_{\text{heat,model}}$.